静岡県立大学大学院薬食生命科学総合学府
博　士　論　文

微粒子設計技術を用いたシクロスポリン A の体内動態制御

Pharmacokinetic control of cyclosporine A with flash nanoprecipitation and powderization technologies

薬物動態学講座
鈴木 寛貴 (Hiroki Suzuki)

2018 年 3 月

微粒子設計技術を用いたシクロスポリン A の体内動態制御

Pharmacokinetic control of cyclosporine A with flash nanoprecipitation and powderization technologies

本論文は静岡県立大学大学院 薬食生命科学総合学府
博士論文である.

2018 年 3 月
(March, 2018)

静岡県立大学大学院 薬食生命科学総合学府
博士後期課程 薬食生命科学専攻 薬物動態学講座

鈴木 寛貴
Hiroki Suzuki

Abbreviations

ASD	Amorphous solid dispersion
ASD/CsA	Amorphous solid dispersion of cyclosporine A
AUC	Area under the curve of plasma concentration *versus* time
BA	Bioavailability
C_{max}	Maximum concentration
CsA	Cyclosporine A
CV	Coefficient of variation
CYP3A4	Cytochrome P450 3A4
DLS	Dynamic light scattering
DMSO	Dimethyl sulfoxide
DSC	Differential scanning calorimetry
ESI	Electrospray ionization
FDA	U.S. Food and Drug Administration
FDD	Fine Droplet Drying
FNP	Flash nanoprecipitation
GI	Gastrointestinal
HPC	Hydroxypropyl cellulose
LSD	Least significant difference
MIVM	Multi-inlet vortex mixer
MS	Mass spectrometry
nCsA	Nanoprecipitated cyclosporine A powder
nCsA/MAN	Nano-matrix formulation of cyclosporine A using mannitol
P-gp	P-glycoprotein
PLM	Polarized light microscopy
RH	Relative humidity
SEM	Scanning electron microscopy
SIR	Selected ion recording
SPAN	Span factor

$T_{1/2}$	Half-life time
T_{max}	Time to reach maximum concentration
UPLC	Ultra performance liquid chromatography
XRPD	X-ray powder diffraction

Contents

Introduction

Over the past few decades, cyclosporine A (CsA), a lipophilic cyclic undecapeptide (Fig. 1), has crucial roles in preventing transplant rejection and treating autoimmune diseases because of its potent immunosuppressive actions [1–3]. CsA was firstly isolated from the fungus *Tolypocladium inflatum* [4], and it can also be obtained *via* biosynthesis [5] or chemical total synthesis [6] at present. Immunosuppressive activity of CsA was discovered in 1976, the mechanism of which is based on the suppression of T-cell-dependent immune reaction *via* calcineurin inhibition [7, 8]. In 1983, CsA was approved as a pharmaceutical agent for prevention of allograft rejection by U.S. Food and Drug Administration (FDA). Currently, CsA has obtained FDA approval for the treatment of various diseases, including rheumatoid arthritis, psoriasis, nephrotic syndrome, and atopic dermatitis [9]. In addition, animal studies and clinical trials have revealed the potential of CsA to treat T-cell large granular lymphocyte leukemia [10], traumatic brain injury [11], ischemic heart disease [12],

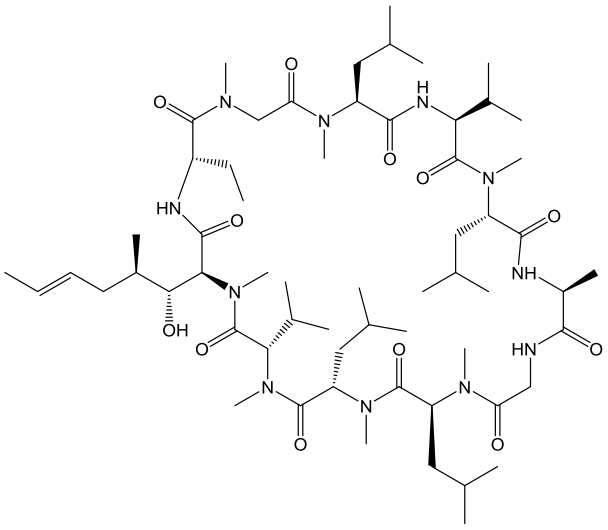

Fig. 1 Chemical structure of cyclosporine A.

and chronic steroid-dependent asthma [13]. However, oral administration of CsA often results in limited absorption with high variability, possibly contributing to insufficient and inconsistent clinical outcomes [14].

Solubility of CsA is as low as ca. 20 μg/mL in water at 25°C [15], and the poor solubility is a causative factor for the undesirable biopharmaceutical properties. Moreover, CsA is a substrate for cytochrome P450 3A4 (CYP3A4) [16] and P-glycoprotein (P-gp) [17], and the systemic exposure of CsA can be reduced by functions of CYP3A4 and P-gp. These factors associated with CsA pharmacokinetics vary depending on diets [18, 19], patient conditions [20–22], and concomitant drugs [23–25] (Table 1). Therefore, large variation in pharmacokinetics of CsA is often observed among individual patients. Immunosuppressive activity of CsA is strongly correlated with the blood concentration [26]. The low concentration of CsA can cause insufficient immunosuppressive actions, leading to organ rejection in transplantation. In clinical practice, the CsA dose is adjusted by monitoring of the blood concentration [26]. However, the dose adjustment has been reported to be sometimes deficient since the limited dissolution rate of CsA arising from low solubility results in an erratic relationship between the administered dose and the systemic exposure [27]. These problems have stimulated efforts to produce improved and predictable pharmacokinetic behavior of CsA [28, 29]. Dissolution process of CsA in gastrointestinal (GI) tract can impact the pharmacokinetic profile after the oral administration [30], and so improvement in CsA dissolution is thought to be essential for the pharmacokinetic control.

To improve the dissolution behavior of CsA, both industrial and academic formulators have extensively investigated and developed many promising CsA formulations employing lipid particles [31–33], polymeric carriers [34–36], and other systems [30, 37, 38] (Table 2). Lipid- and polymer-based formulations can increase apparent solubility of CsA, improving the oral absorption [31–36]. Nevertheless, there are several disadvantages and

Table 1 Factors influencing pharmacokinetics of CsA in human

	Mechanisms for the pharmacokinetic change	Effects on the pharmacokinetic behavior	References
Diets			
High-fat meals	Solubilization of CsA	Increase of AUC by 376% in healthy volunteers	[18]
Flavonoids	Inhibition of CYP3A4	Increase of C_{max} and AUC by 150% and 186%, respectively, in healthy volunteers	[19]
Patient conditions			
Aging	Increase in lipoprotein concentration Impairment of liver function	Decrease of CL by 37% in marrow transplant patients (below 10 yeas vs. above 40 years)	[20]
Diabetes	Induction of CYP3A4 Delay of gastric emptying rate Glycation of albumin	Decrease of C_{max} and AUC by 86% and 81%, respectively, in children with type I diabetes	[21]
GI inflammation	Inhibition of P-gp	Increase of C_{max} and AUC by 164% and 171%, respectively, in marrow transplant patients	[22]
Concomitant drugs			
Metoclopramide	Acceleration of gastric emptying rate	Increase of C_{max} and AUC by 124% and 122%, respectively, in kidney transplant patients	[23]
Telaprevir	Inhibition of CYP3A4	Increase of AUC by 460% in healthy volunteers	[24]
Rifampicin	Induction of CYP3A4	Decrease of AUC by 27% in healthy volunteers	[25]

AUC, area under the curve of plasma concentration *versus* time; CL, clearance; C_{max}, maximum concentration; CsA, cyclosporine A; CYP3A4, cytochrome P450 3A4; GI, gastrointestinal; and P-gp, P-glycoprotein.

limitations in the use of these solubilization technologies [39]. These formulations normally show low physicochemical stability, restricted incorporation capacity of a drug, complexity of manufacture, and high production cost. According to the Noyes-Whitney equation and Prandtl equation, the dissolution rate of poorly-soluble drugs can be increased by reducing particle size [40, 41]. Particle size reduction is a simple and cost-effective approach [42] and may be effective to improve dissolution behavior of CsA.

The approaches for production of fine particles can be divided into top-down and bottom-up processes [43, 44]. Top-down methods are essentially high energy processes, and drug particles are broken down to lower size. Top-down is an easy and feasible approach for particle size reduction, whereas it has some limitations, including inefficiency of particle size reduction and broad particle size distribution of prepared particles [45]. In contrast, bottom-up methods are low energy processes and has the potential to produce particles with narrow size distribution [42]. However, the particle size of drug particles obtained by conventional bottom-up is relatively larger than that of particles prepared by top-down [46]. Flash nanoprecipitation (FNP) technology using a multi-inlet vortex mixer (MIVM) and Fine Droplet Drying (FDD) process employing inkjet head have been proposed as novel bottom-up methods for preparation of fine particles with narrow size distribution [47, 48]. These novel technologies have the high potential to generate fine particles of CsA with modified physicochemical properties. However, far less is known about these feasibilities to provide desirable oral absorption of CsA.

The present study aimed to control pharmacokinetic behavior of CsA by modification of the physicochemical properties. In chapter 1, nano-matrix formulation of CsA was prepared with a combined use of FNP using MIVM and spray-drying to produce the rapid oral absorption. The physicochemical properties of CsA formulations were evaluated in terms of appearance, crystallinity, re-dispersibility, and dissolution behavior. Pharmacokinetic study

in rats was also conducted after oral administration of the CsA formulations. In chapter 2, amorphous solid dispersion (ASD) of CsA was prepared by FDD process employing inkjet head to obtain improved pharmacokinetic property of CsA. The physicochemical properties were characterized with a focus on appearance, particle size distribution, bulk density, flowability, crystallinity, dissolution behavior, and stability under accelerated conditions. Pharmacokinetic behavior of CsA in rats was also clarified after oral administration of CsA samples.

Table 2 Literature-based oral formulations of CsA

Formulation systems	Main features	Pharmacokinetic parameters	References
Lipid particles			
DHA-microemulsion	Encapsulation of drug into emulsion Inhibition of CYP3A activity by DHA	C_{max}: 1.1-fold ↑ ; AUC: 1.1-fold ↑ (vs. Neoral®) in rats	[31]
OACS-coated liposome	Encapsulation of drug into liposome Cell-penetrating property of OACS	C_{max}: 3.8-fold ↑ ; AUC: 3.2-fold ↑ (vs. pure CsA®) in rats	[32]
Bilosome containing gelatin	Cell-penetrating property of bilosome Protection of bilosome by gelatin	C_{max}: 1.3-fold ↑ ; AUC: 1.7-fold ↑ (vs. Neoral®) in dogs	[33]
Polymeric particles			
Soluplus®-based polymeric micelle	Encapsulation of drug into micelle	C_{max}: 1.3-fold ↑ ; AUC: 1.3-fold ↑ (vs. Neoral®) in rats	[34]
Eudragit® S100-based nanoparticles	Incorporation of drug into polymeric particles pH-Sensitive drug release by Eudragit® S100	C_{max}: 1.7-fold ↑ ; AUC: 1.3-fold ↑ (vs. Neoral®) in rats	[35]
Poly[MPC-*co*-BMA]-based self-micellizing solid dispersion	High self-micellizing potency of poly[MPC-*co*-BMA] High stability of the solid dispersion focusing on dissolution property	C_{max}: 11-fold ↑ ; AUC: 45-fold ↑ (vs. amorphous CsA) in rats	[36]

Table 2 (Continued)

Formulation systems	Main features	Pharmacokinetic parameters	References
Other systems			
DM-β-CyD complex	Inclusion of drug into cyclodextrin complex	C_{max}: 2.8-fold ↑ ; AUC: 4.7-fold ↑ (vs. pure CsA®) in rats	[37]
mPEG conjugate	Increase in water solubility of drug by mPEG conjugation	C_{max}: 1.6-fold ↑ ; AUC: 1.5-fold ↑ (vs. amorphous CsA) in rats	[38]
HPC-SSL-based amorphous solid dispersion	Supersaturation by amorphization of drug Increase in wettability by HPC-SSL	C_{max}: 5.1-fold ↑ ; AUC: 5.2-fold ↑ (vs. amorphous CsA) in rats	[30]

AUC, area under the curve of plasma concentration *versus* time; BMA, butyl methacrylate; C_{max}, maximum concentration; DM-β-CyD, dimethyl-β-cyclodextrin; DHA, docosahexaenoic acid; HPC-SSL, hydroxypropyl cellulose-SSL; MPC, 2-methacryloyloxyethyl phosphorylcholine; mPEG, monomethoxy polyethylene glycol; and OACS, *N*-octyl-*N*-arginine-chitosan.

Chapter 1. Nano-matrix oral formulation of cyclosporine A prepared with flash nanoprecipitation technology using multi-inlet vortex mixer

1-1. Background

Particle size reduction leads to increase of effective surface area and decrease of diffusion layer thickness of drug particles, accelerating the dissolution rate [49, 50]. Therefore, an application of nanotechnology to poorly-soluble drugs has attracted much attention to improve their dissolution behavior. FNP technology has been developed for preparation of nanoparticles with narrow size distribution [51, 52]. FNP can control kinetic processes including micromixing and stabilizer adsorption. Rapid micromixing of solvent and anti-solvent results in supersaturation of drugs, inducing high nucleation rate for rapid precipitation of nanoparticles. The rapid and diffusion-limited aggregation is arrested by stabilizer adsorption on the surface of particles, contributing to control of particle size and stable generation of nanoparticles [47]. Four-stream MIVM can produce rapid and homogeneous mixing by infusion of separate solvent or anti-solvent from four inlets, rapidly precipitating nanoparticles with narrow size distribution [53, 54]. These findings prompted us to develop CsA nanoparticles by FNP process using MIVM for improvement in the oral absorption.

In this chapter, for enhancement in oral absorption of CsA, two types of CsA powders were prepared by combination of FNP and spray-drying; nanoprecipitated CsA powder (nCsA) and nano-matrix formulation of nanoprecipitated CsA using mannitol (nCsA/MAN) as a matrix former. The physicochemical properties of both CsA spray-dried particles were characterized, and pharmacokinetic study in rats was also carried out to clarify the oral absorption of CsA after oral administration of CsA samples.

1-2. Materials and methods

1-2-1. Chemicals

Amorphous CsA was purchased from Changzhou An-Yuan Import and Export Corporation (Changzhou, China). Crystalline CsA was obtained by preparing a saturated solution of CsA in acetone and storing at –20°C, and the crystals were collected by filtration from the cold acetone solution. Soy bean lecithin and α-lactose monohydrate were bought from Cargill Texturizing Solutions (Wayzata, USA) and Friesland Campina Domo (Amersfoort, Netherlands), respectively. Mannitol was kindly supplied by Pharmaxis (Frenchs Forest, Australia). All other chemicals were purchased from commercial sources.

1-2-2. Preparation of nCsA and nCsA/MAN

A nanosuspension of CsA was produced by FNP approach using MIVM (Fig. 2A), followed by spray-drying to obtain nCsA and nCsA/MAN (Fig. 2B). Briefly, CsA was dissolved in ethanol at a concentration of 50 mg/mL (Solution I). Lecithin and lactose as stabilizers were dissolved in water at 0.125 mg/mL and 5 mg/mL, respectively (Solution II). Solution I was loaded into two syringes, and solution II was also loaded into two other syringes at the same volume. All four syringes were connected to the MIVM with each dispensing 20 mL at 30 mL/min. Micromixing and nanoparticle precipitation occurred inside the mixing chamber. The products were collected from the MIVM into a beaker with 400 mL of deionized water stirred with a magnetic stirrer at 650 rpm. The suspension was divided into two equal portions by volume, and mannitol was added into one suspension with a mass loading equal to the CsA. Each suspension was refrigerated for at least 2 h and then spray-dried using a Büchi Mini Spray-Dryer B-290 (Büchi Labortechnik, Flawil, Switzerland) connected to a Büchi Dehumidifier B-296 (in open loop, blowing mode) under the following

(A)

(B)

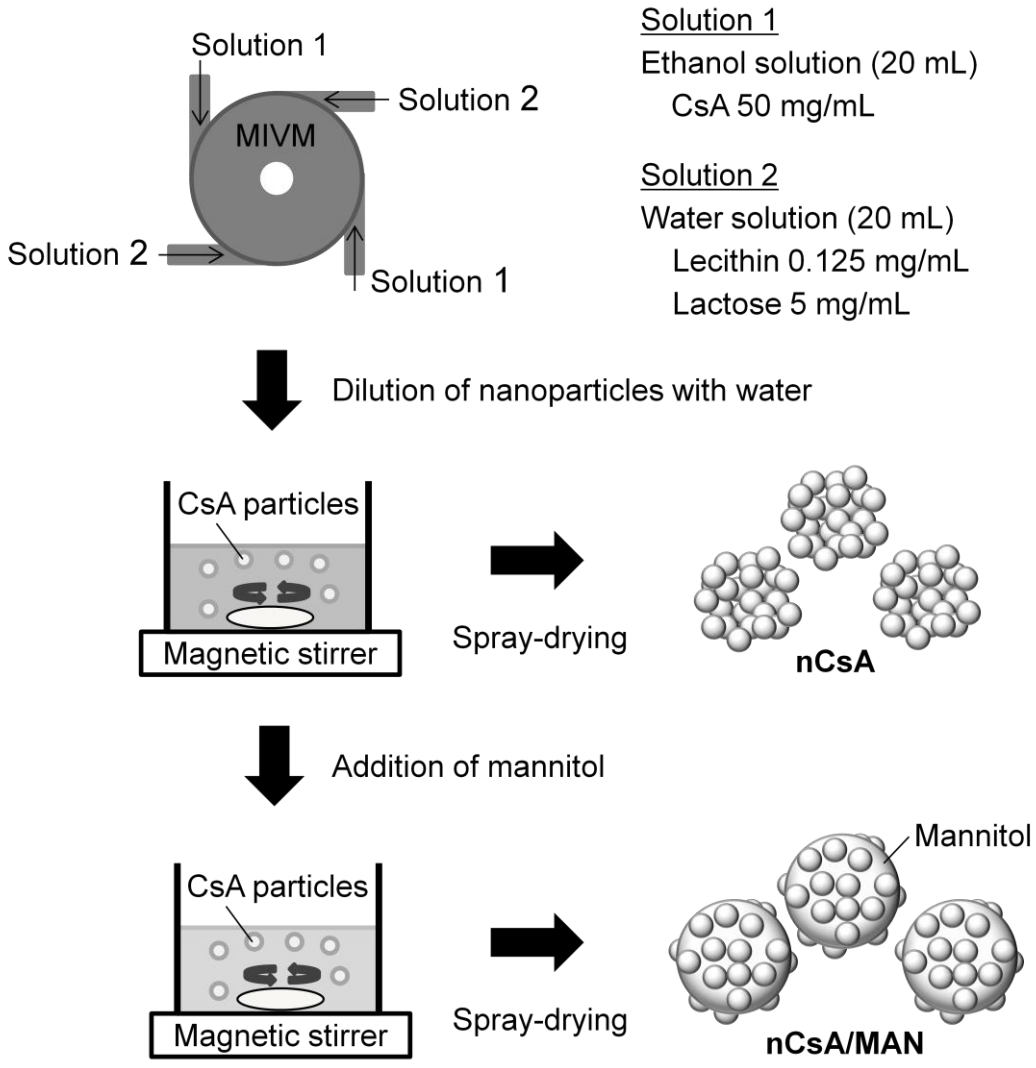

Fig. 2 Schematic illustrations. (A) Structural configuration of MIVM. Bar represents 5 cm. (B) Preparation procedure of nCsA and nCsA/MAN.

conditions: inlet temperature of 120°C, outlet temperature of 70–89°C, aspiration rate of 100%, atomizing air flow at 880 L/h, and liquid feed rate of 3.5 mL/min. The powders from the collector were transferred to separate sealed containers and stored with silica gel desiccant at 22°C until further analysis and processing.

The amount of CsA in the spray-dried powders was determined using a Waters Acquity ultra performance liquid chromatography equipped with electrospray ionization mass spectrometry (UPLC/ESI-MS) system (Waters, Milford, Massachusetts), including a binary solvent manager, column compartment, sample manager, column compartment, and SQD connected with the MassLynx software. Acquity UPLC BEH C18 column (particle size: 1.7 μm, column size: 2.1 mm × 50 mm; Waters) was used at 65°C. Acetonitrile (A) and 5 mM ammonium acetate (B) were selected as a mobile phase for the separation of CsA. The flow rate of mobile phase was 0.25 mL/min, and the gradient condition was set as follows: 0–1.0 min, 50% A; 1.0–3.0 min, 50–95% A; 3.0–3.5 min, 95% A; and 3.5–4.0 min, 50% A. Analysis was carried out using selected ion recording (SIR) for specific m/z 1203 for CsA $[M+H]^+$.

1-2-3. Dynamic light scattering (DLS)

The particle size of nCsA and nCsA/MAN re-suspended in distilled water was measured with DLS using Malvern Zetasizer Nano ZS (Malvern, Worcestershire, UK). Span factor (SPAN) was calculated as SPAN = $(d_{90} - d_{10})/d_{50}$, and the d_{10}, d_{50}, and d_{90} are the particle diameters at 10%, 50%, and 90% of cumulative volume, respectively.

1-2-4. Scanning electron microscopy (SEM)

The morphology of CsA samples was visualized with SEM, Miniscope® TM3030 (Hitachi, Tokyo, Japan). CsA samples were fixed on an aluminum sample holder with

double-sided carbon tape, and platinum was coated over the CsA samples using a magnetron sputtering device, MSP-1S (Vacuum Device, Ibaraki, Japan).

1-2-5. X-ray powder diffraction (XRPD)

XRPD patterns were collected using a Mini Flex II (Rigaku, Tokyo, Japan) with Cu Kα radiation generated at 40 mA and 35 kV. The determination of CsA samples was carried out within an angular range of 3–40° (2θ) at a step size of 0.2° and scanning speed of 2°/min.

1-2-6. Differential scanning calorimetry (DSC)

A DSC Q 1000 (TA Instruments, New Castle, DE, USA) was used for DSC analysis, and the DSC thermograms were collected in an aluminum close-pan system. The operation conditions were set as follows: sample weight of ca. 3 mg, heating rate of 5°C, and nitrogen purge at 70 mL/min. The calibration of temperature axis was carried out with indium (ca. 5 mg, 99.999% pure, onset at 156.6°C).

1-2-7. Dissolution test

Dissolution testing on CsA samples was performed in 100 mL of distilled water. The dissolution medium was stirred at 50 rpm using a magnetic stirrer SST-66 (Shimadzu, Kyoto, Japan) at 37°C. CsA samples (ca. 2 mg-CsA) were weighed and added into the glass beaker with 100 mL of water. Samples (400 μL) were collected and centrifuged at 10,000 rpm for 5 min. To determine CsA concentration, the supernatants diluted with acetonitrile were subjected to UPLC analysis as described in section 1-2-2.

1-2-8. Pharmacokinetic study

Male sprague-dawley rats, weighing 200–300 g (6–8 weeks of age; Japan SLC,

Shizuoka, Japan), were housed three per cage with free access to food and water, and the room was maintained on a 12-h dark/light cycle with controlled temperature (24±1°C) and humidity (55±5%). Rats were fasted for at least 12 h before oral administration of CsA samples. The pharmacokinetic study was conducted in accordance with guidelines approved by the Institutional Animal Care and Ethical Committee of the University of Shizuoka.

Each CsA sample was suspended in 1 mL of distilled water, and it was orally administered at a dose of 10 mg-CsA/kg in rats. CsA was dissolved in dimethyl sulfoxide (DMSO), and the CsA solution at a dose of 0.5 mg/kg was intravenously administered in rats to calculate oral bioavailability (BA) of CsA samples. After administration of CsA samples, 400 μL of blood samples was collected from the tail veins of rats at various periods. The collected blood samples were centrifuged at 10,000×*g* for 10 min, and the supernatants were stored below –20°C until analysis. The plasma concentration of CsA was monitored by UPLC analysis as described in section 1-2-2 with some modifications. Briefly, 150 μL of acetonitrile solution including tamoxifen, an internal standard material, was added to 50 μL of plasma sample for removal of protein in plasma samples, and its sample was centrifuged at 2,000×*g* for 5 min. The supernatant was filtrated through a 0.2-μm filter and was analyzed by an internal standard method using the UPLC system. Peaks for tamoxifen and CsA were detected at the retention times of 2.25 and 3.02 min, respectively. Analysis was carried out using SIR for specific m/z 372 for tamoxifen $[M+H]^+$ and 1203 for CsA $[M+H]^+$. The UPLC method for determination of CsA was validated in terms of linearity, accuracy, precision, and assay recovery according to International Conference on Harmonization of Technical Requirements for Registration of Pharmaceuticals for Human Use guidelines "Q2B Validation of Analytical Procedures: Methodology". At the concentrations of 10 and 1,000 ng/mL, the observed recovery of CsA was 97.3–100.9%. The pharmacokinetic parameters for CsA were calculated by means of non-compartment methods using the WinNonlin

program (Ver. 4.1, Pharsight Corporation, Mountain View, CA). Oral BA was calculated as BA = $D_{i.v.}$×$AUC_{p.o.}$/$D_{p.o.}$×$AUC_{i.v.}$. $D_{i.v.}$ and $D_{p.o}$ are dose of intravenous and oral administration, respectively. $AUC_{i.v.}$ and $AUC_{p.o.}$ are $AUC_{0-inf.}$ after intravenous and oral administration, respectively. To estimate the variation of CsA absorption after oral administration of CsA samples, coefficient of variation (CV) in $AUC_{0-inf.}$ was defined as CV = standard deviation/mean and calculated.

1-2-9. Statistical analysis

For statistical comparisons, one-way analysis of variance with pairwise comparison by Fisher's least significant difference (LSD) procedure was used (Statcel3, The Publisher OSM Ltd., Saitama, Japan). A P value of < 0.05 was considered significant for all analyses.

1-3. Results and discussion

1-3-1. Size of CsA particles in suspension

In the present study, CsA nanoparticles were obtained by FNP with MIVM, and the particle size was measured by DLS analysis (Table 3). The median size of CsA particles was found to be ca. 170 nm. FNP using MIVM could produce CsA nanoparticles with narrow size distribution as evidenced by 1.0 of SPAN. Although slight increase in the median size was observed at 5 h after preparation of CsA nanoparticles, they kept nanoscale particle size. In general, Ostwald ripening occurs for nanosuspensions [55]. Smaller particles with enhanced dissolution rate shrink by their dissolution, and subsequently the dissolved drugs precipitate on the surface of larger particles. The rate of this process is dependent on the uniformity of the particle size. The narrow size distribution of CsA nanoparticles could contribute to the limited increase in median size of CsA nanoparticles in suspension. Lecithin has been reported to inhibit particle aggregation by the electronic and steric stabilization [56], and so the action of lecithin could also result in high colloidal stability of CsA nanoparticles. On the basis of the result from DLS analysis, the MIVM successfully generated CsA nanoparticles.

Table 3 Size distribution of CsA nanoparticles in suspension

Time after FNP process	d_{10} (nm)	d_{50} (nm)	d_{90} (nm)	SPAN
T = 0 h	146	169	319	1.0
T = 5 h	180	221	496	1.4

The d_{10}, d_{50}, and d_{90} are the particle diameters at 10%, 50%, and 90% of cumulative volume, respectively. SPAN = $(d_{90} - d_{10})/d_{50}$. CsA suspension was stored at room temperature, and DLS analysis on CsA suspension was conducted at 0 h or 5 h after FNP process.

(A)

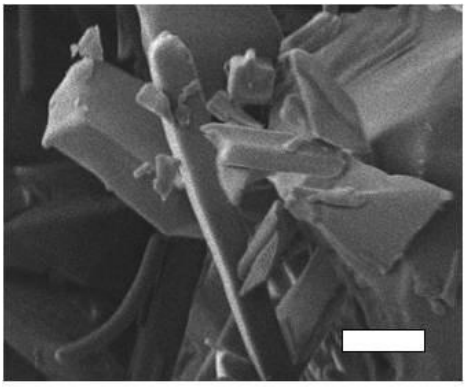

(B)

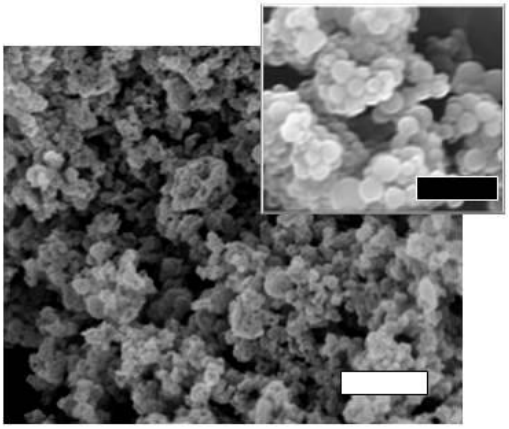

(C)

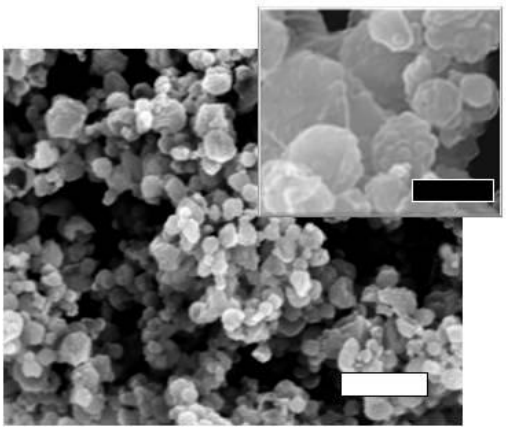

Fig. 3 SEM images of CsA samples, including (A) amorphous CsA, (B) nCsA, and (C) nCsA/MAN. The inserts highlight the surface of each CsA powder. White and black bars represent 5 and 0.5 μm, respectively.

1-3-2. Morphology of spray-dried CsA particles

CsA nanosuspension with or without mannitol was spray-dried for preparation of nCsA/MAN or nCsA, respectively. Their morphologies were visualized by SEM observation (Fig. 3). On the basis of the SEM image, amorphous CsA was irregular-shaped powders with average particle size of ca. 60 μm (Fig 3A). On the other hand, the nCsA existed as micron-sized aggregates of CsA nanoparticles (Fig. 3B). The size of primary particles in nCsA appeared to be ca. 200 nm and is almost consistent with the result from DLS analysis. nCsA/MAN existed as micron-sized aggregates of CsA nanoparticles embedded in mannitol-based matrix (Fig. 3C). As the droplets shrunk during spray-drying, the CsA nanoparticles clustered together to form the micron-sized aggregates. Simultaneously, mannitol came out of solution and could form a matrix phase among CsA nanoparticles.

1-3-3. Crystallinity of CsA in spray-dried CsA particles

XRPD and DSC analyses were conducted to clarify the crystallinity of CsA in nCsA and nCsA/MAN (Fig. 4). In the XRPD pattern of crystalline CsA, several intense peaks were observed (Fig. 4A), and their peaks indicated a tetragonal crystal form [57]. In contrast, there were no peaks attributable to crystalline CsA for amorphous CsA, nCsA, and nCsA/MAN, suggesting that CsA in both spray-dried particles existed in an amorphous state. Mannitol was the crystalline β-form as evidenced by the XRPD pattern, whereas the XRPD pattern of nCsA/MAN appeared to be partially different from that of mannitol. There is crystal polymorph of mannitol including α-, β-, and δ-form [58], and so nCsA/MAN would contain different crystal form of mannitol. The DSC thermograms of these samples were also analyzed to further characterize the physical state of spray-dried particles (Fig. 4B). The endothermic peak of crystalline CsA was observed at 105°C. No thermal event occurred at 105°C for amorphous CsA, and the endothermic peak was shifted to 125°C. It

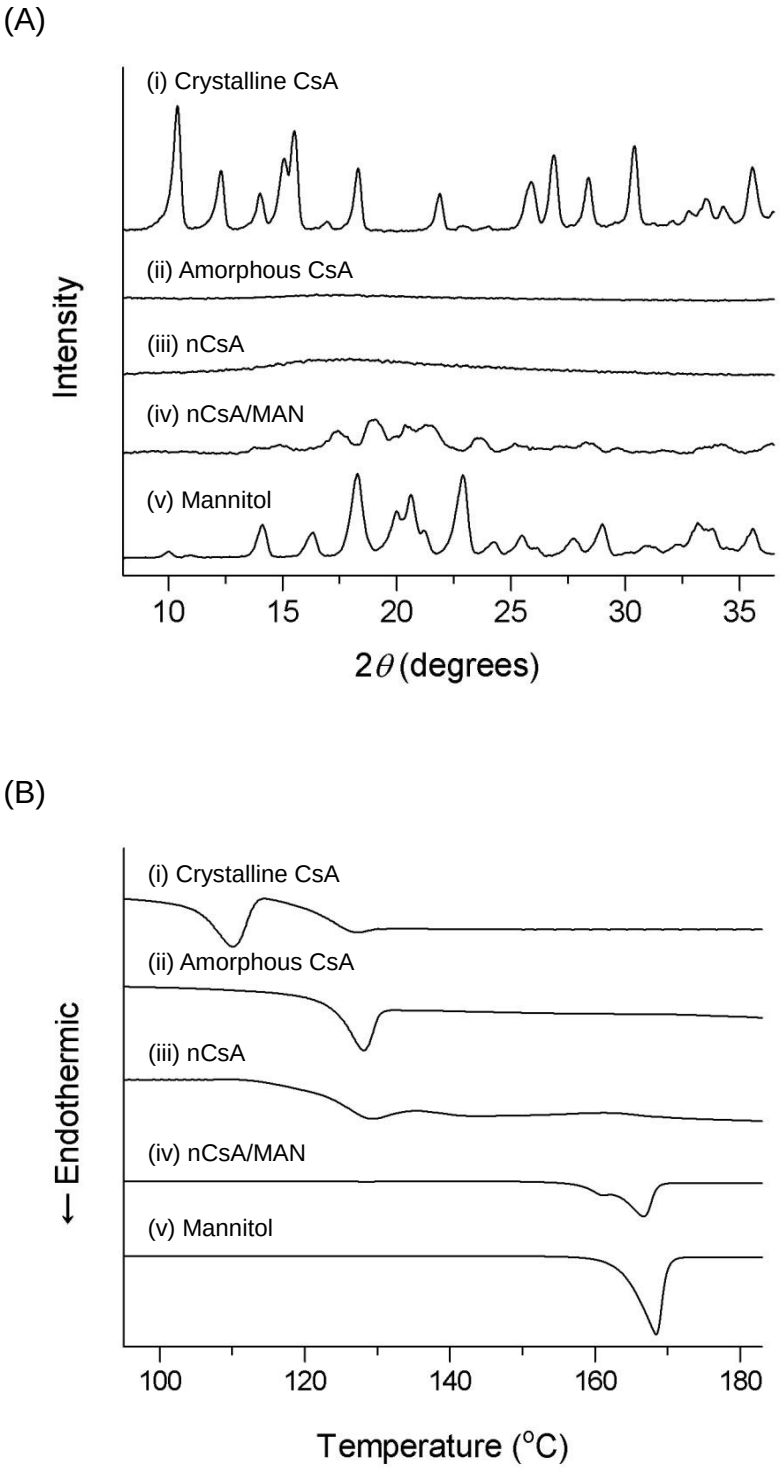

Fig. 4 Crystallinity of CsA in spray-dried particles. (A) XRPD patterns and (B) DSC thermograms of (i) crystalline CsA, (ii) amorphous CsA, (iii) nCsA, (iv) nCsA/MAN, and (v) mannitol.

has been reported that CsA forms thermotropic liquid crystals at over 120°C [59], and so the peak shift could be explained by the phase transition of CsA. The phase transition appeared to occur for nCsA because the nCsA showed the endothermic peak at 125°C. However, these peaks were absent for nCsA/MAN. Mannitol phase might prevent molecular mobility by interactions of mannitol and CsA, possibly resulting in inhibition of the phase transition of CsA during thermal analysis. Mannitol produced a melting endotherm at 165°C. On the other hand, nCsA/MAN exhibited two endothermic peaks, and the peaks were observed at 160°C and 165°C. Spray-drying of mannitol alone results in β-form of mannitol, whereas co-spray-drying of mannitol and compounds produces α-form of mannitol [60]. In the present study, mannitol was spray-dried with CsA nanoparticles, and so mannitol could exist in crystalline α- and β-forms.

1-3-4. Size distribution of re-dispersed CsA particles

Particle size of nCsA and nCsA/MAN re-suspended in distilled water was measured by DLS analysis (Fig. 5). In distilled water, both nCsA and nCsA/MAN could reconstitute nanoparticles with 317 and 298 nm of median size, respectively. Particle size distribution of nCsA/MAN was narrower than that of nCsA, and SPAN of nCsA and nCsA/MAN was calculated to be 1.3 and 1.2, respectively. The median size and SPAN of nCsA/MAN were subtly lower than those of nCsA, demonstrating the slightly high re-dispersibility of nCsA/MAN. Mannitol phase inhibits the particle contacts during drying process and furthermore improves the wettability of drug particles [46]. Therefore, use of mannitol as a matrix former could lead to the high re-dispersibility of nCsA/MAN. The better dispersibility of nCsA/MAN could contribute to improved dissolution behavior of CsA.

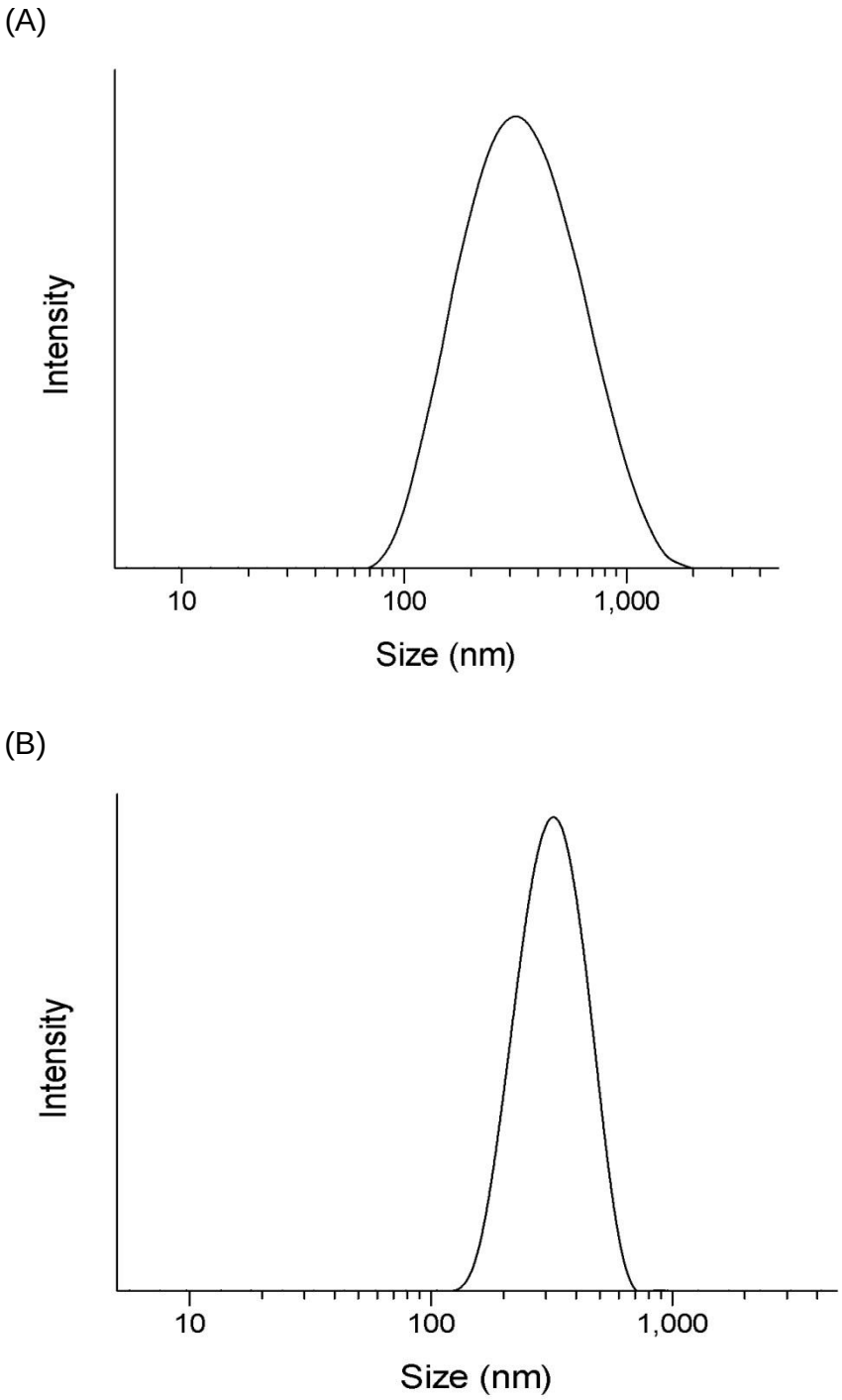

Fig. 5 Size distribution of (A) nCsA and (B) nCsA/MAN re-suspended in distilled water.

1-3-5. Dissolution behavior of spray-dried CsA particles

The dissolution property of CsA samples in water was evaluated up to 60 min to verify improvement in the dissolution behavior of CsA upon FNP approach (Fig. 6). For amorphous CsA, limited dissolution behavior of CsA was observed. In contrast, both nCsA and nCsA/MAN improved dissolution behavior of CsA in distilled water. In comparison with amorphous CsA, nCsA and nCsA/MAN provided 31- and 41-fold increased drug release at 60 min, respectively. The SEM experiment demonstrated the difference in particle size of amorphous CsA and both spray-dried CsA particles, and furthermore DLS data indicated that both spray-dried CsA particles could reconstitute nanoparticles in water. From these outcomes, particle size reduction approach could lead to better dissolution profile of CsA due to increased surface area and decreased diffusion layer of drug particles. The significantly improved drug release was observed for nCsA/MAN compared with nCsA ($P < 0.05$). The enhanced drug release could be attributed to increased wettability and dispersibility of nCsA/MAN. Drugs with solubility lower than 100 μg/mL often show dissolution-limited absorption after their oral administration [61, 62]. Oral absorption of CsA is thought to be highly limited due to poor dissolution rate arising from the low solubility. The accelerated dissolution of CsA from nCsA and nCsA/MAN might contribute to rapid oral absorption of CsA.

1-3-6. Pharmacokinetic behavior of spray-dried CsA particles

Pharmacokinetic behavior of CsA in rats was evaluated after oral administration of CsA samples at a dose of 10 mg-CsA/kg (Fig. 7 and Table 4). Oral administration of amorphous CsA resulted in poor systemic exposure as evidenced by 0.4 μg/mL and 4.1 μg·h/mL of C_{max} and of $AUC_{0-inf.}$ values, respectively. In contrast, enhanced systemic exposure was observed for both nCsA and nCsA/MAN as compared to amorphous CsA, and

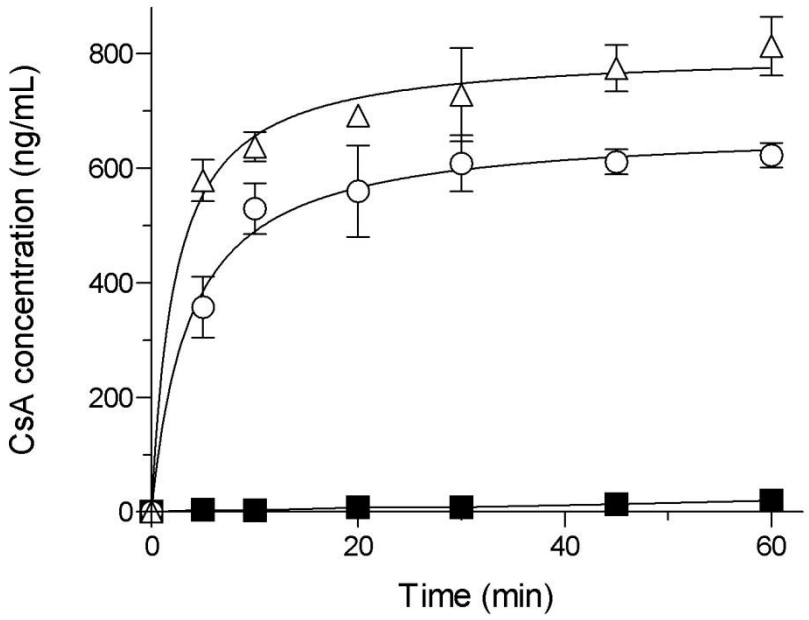

Fig. 6 Dissolution behavior of CsA samples, including amorphous CsA (■), nCsA (○), and nCsA/MAN (△), in distilled water. Data represent mean±S.E. of 3 experiments.

the $AUC_{0-inf.}$ values of nCsA and nCsA/MAN were 12.1 and 12.2 μg·h/mL, respectively. Oral BA of amorphous CsA, nCsA, and nCsA/MAN was calculated to be 4.6, 13.5, and 13.7%, respectively. Thus, the improvement in dissolution behavior of CsA by FNP resulted in ca. 3-fold enhancement in BA of CsA. Interestingly, nCsA/MAN showed faster oral absorption than nCsA, as evidenced by T_{max} values of ca. 3 and 7 h, respectively. Inter-individual variability in systemic exposure of CsA was much lower for nCsA/MAN (CV in $AUC_{0-inf.}$: 11.5%) than nCsA (CV in $AUC_{0-inf.}$: 55.0%). The nCsA mainly consisted of CsA, and low solubility of CsA might result in re-precipitation of dissolved drug in GI tract. In contrast, the mannitol in nCsA/MAN might inhibit the re-precipitation by interactions of mannitol and CsA, possibly contribute to stable dissolution of CsA in GI tract. The narrow

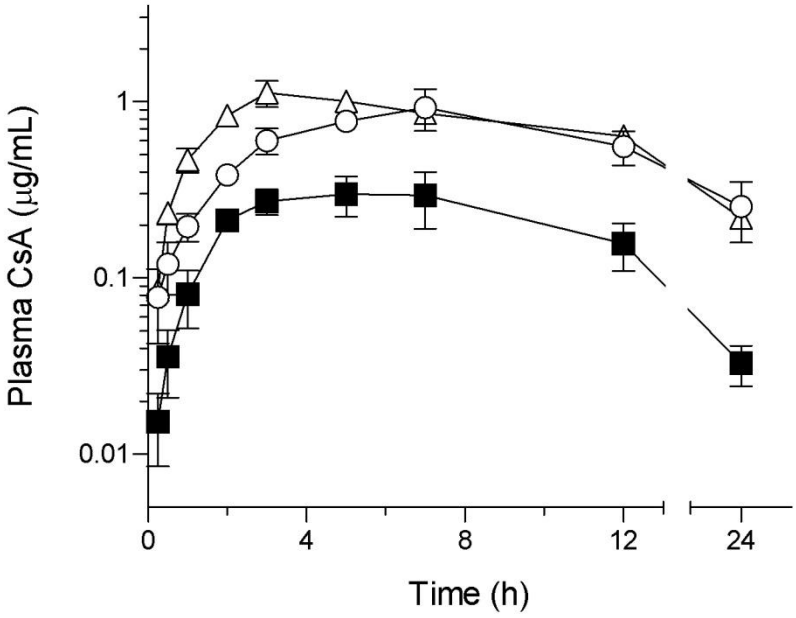

Fig. 7 Plasma concentration-time profiles of CsA after oral administration of CsA samples (10 mg-CsA/kg) in rats. ■, amorphous CsA; ○, nCsA; and △, nCsA/MAN. Data represents mean±S.E. of 4–5 experiments.

size distribution of nCsA/MAN might lead to the less aggregability compared with nCsA. Therefore, combined use of FNP process using MIVM and mannitol-based matrix approach could lead to enhanced oral absorption of CsA with low variability.

Table 4 Pharmacokinetic parameters of CsA after administration of CsA samples

	C_{max} (μg/mL)	T_{max} (h)	$AUC_{0-inf.}$ (μg· h/mL)	BA (%)
Amorphous CsA	0.4±0.1	4.8±1.1	4.1±1.0	4.6
nCsA	0.9±0.2*	7.0±0.5	12.1±3.3*	13.5
nCsA/MAN	1.0±0.1*	3.8±0.4$^{\#}$	12.2±0.1*	13.7

C_{max}, maximum concentration; T_{max}, time to reach maximum concentration; AUC_{0-inf}, area under the curve of plasma concentration *versus* time from t=0 to t=infinity; and BA, bioavailability. Data represents mean±S.E. of 4–5 experiments. *, $P<0.05$ and $^{\#}$, $P<0.05$ with respect to amorphous CsA and nCsA, respectively.

1-4. Conclusion

FNP process using MIVM successfully produced CsA nanoparticles with narrow size distribution. Re-suspended nCsA and nCsA/MAN could reconstitute CsA nanoparticles in distilled water, leading to rapid dissolution of CsA. In comparison with nCsA, nCsA/MAN improved dissolution behavior of CsA. Orally-dosed nCsA and nCsA/MAN provided high systemic exposure of CsA in rats compared with amorphous CsA. Although nCsA enhanced oral absorption of CsA, there was slow absorption of CsA with large variability for nCsA. In contrast, oral administration of nCsA/MAN resulted in rapid elevation of plasma CsA concentration and the consistent systemic exposure. From these findings, nCsA/MAN might improve CsA pharmacological actions because of its rapid and stable oral absorption.

Chapter 2. Amorphous solid dispersion of cyclosporine A prepared by Fine Droplet Drying process

2-1. Background

Particle size and the size distribution are critical factors influencing absorption property of poorly-soluble drugs [63, 64]. A new powderization technology employing inkjet head, define as FDD process, has been proposed for preparation of powder formulations with uniform shape and size [65]. FDD process includes steps of droplet formation and drying. For the droplet formation, the inkjet head enables continuous generation of fine droplets with narrow size distribution because of the capacity to supply high frequency, contributing to preparation of powder formulations with desirable particle size. ASD technology has been widely applied to poorly-soluble drugs since it is an efficacious approach for improvement their dissolution behavior [66, 67]. Therefore, a strategic application of FDD process to preparation method of ASD formulation may lead to desirable pharmacokinetics of CsA.

In this chapter, ASD formulation of CsA (ASD/CsA) was prepared by FDD process for improvement in oral absorption of CsA. The physicochemical properties were characterized in terms of morphology, particle size distribution, flowability, crystallinity, dissolution behavior in distilled water, and physicochemical stability under accelerated conditions. Pharmacokinetic behavior of CsA in rats was also investigated after oral administration of ASD/CsA to clarify the possible enhancement absorption by the ASD approach.

2-2. Materials and methods

2-2-1. Chemicals

Amorphous CsA was kindly supplied by ILS Inc. (Ibaraki, Japan). Crystalline CsA was obtained by preparing a saturated solution of CsA in acetone and storing at –20°C, and the crystals were collected by filtration from the cold acetone solution. Hydroxypropyl cellulose (HPC)-SSL, 1,4-dioxane, and ammonium acetate were purchased from Wako Pure Chemical Industries (Osaka, Japan). Acetonitrile (HPLC grade) was bought from Kanto Chemical (Tokyo, Japan). All other reagents were purchased from commercial sources.

2-2-2. Preparation of ASD/CsA

In the present study, HPC-SSL was used for an ASD/CsA, and the FDD process using RICOH MH2420, an inkjet head, was conducted for preparation of the ASD/CsA (Fig. 8). Briefly, CsA (100 mg) and HPC-SSL (1,900 mg) were dissolved in 1,4-dioxane. The 1,4-dioxane is a volatile solvent and can completely dissolve both CsA and HPC-SSL, and therefore it was employed as a solvent in the present study. The solute concentration was 2% (w/v) to stably generate uniform droplets by atomization, and the solution was mixed for 1 h under constant stirring of 1,000 rpm using a magnetic stirrer (AS ONE, Osaka, Japan), followed by filtration through a 1-μm filter. The filtered solution was fed at feed rate of 3 g/min into drying chamber using RICOH MH2420 with nozzle hole diameter of 8 μm. The atomized solution was dried with dry air. The dried particles were collected by cyclone separator into collection device. For the FDD process, the typical process parameters were frequency of piezo element, air flow temperature, and air flow rate, and these parameters were 310 kHz, 24°C, and 50 m^3/h, respectively.

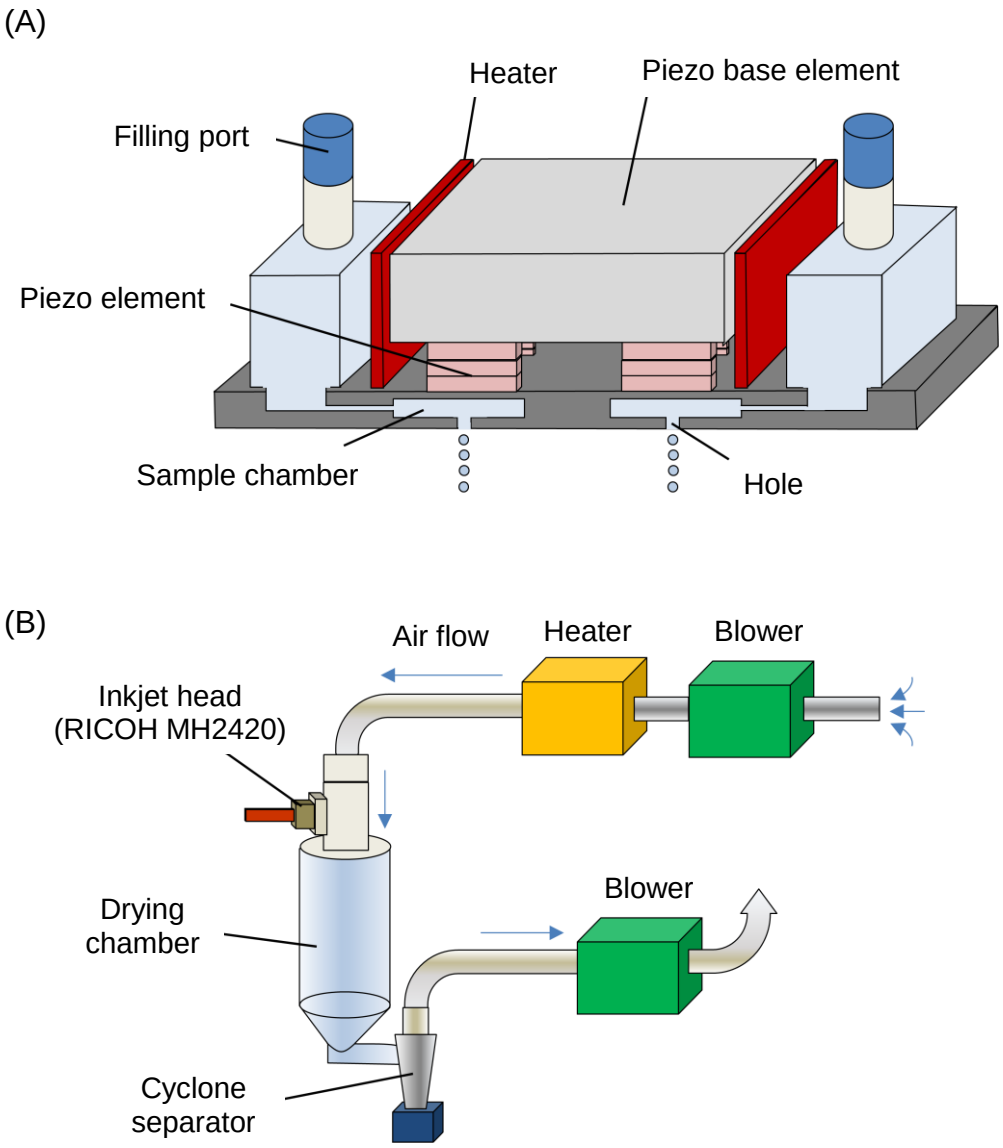

Fig. 8 Schematic illustrations. (A) Structural configuration of RICOH MH2420 and (B) scheme of FDD process.

Spray-dried ASD formulation of CsA was also prepared as a reference formulation. Spray-drying was performed using 2-fluid nozzle as an atomizer and Pulvis Mini Spray GS310 (Yamato Scientific Co., Ltd, Tokyo, Japan) under the following conditions: spray pressure of 0.09 MPa, feeding rate of 3 mL/min, air flow temperature of 45°C, and air flow rate of 40 m^3/h. The amount of CsA in the obtained formulation was determined by UPLC analysis as described in section 1-2-2.

2-2-3. SEM

The morphology of amorphous CsA and ASD/CsA was visualized with SEM as described in section 1-2-4.

2-2-4. Laser diffraction

The particle size of ASD formulations was measured by laser diffraction analysis with Microtrac MT3000II (MicrotracBel, Osaka, Japan).

2-2-5. Bulk density

Graduated cylinder was employed to measure the bulk density of ASD formulations. Sample powders (ca. 1.5 g) were gently introduced into 10 mL of cylinder. After 10 min, the graduated unit of cylinder (*V*) was read, and the bulk density was calculated using the formula weight of powder samples (g)/*V* (mL).

2-2-6. Powder flowability

Powder flowability of ASD formulations was determined using flowability tester (DIT Co. Ltd., Osaka, Japan). The sample powders were moved in the tester by vertical vibration and were collected from the outlet. The amount of collected samples was recorded with time, and the transfer rate (mg/s) was measured and treated as the powder flowability.

2-2-7. XRPD

XRPD pattern was collected using a Mini Flex II (Rigaku, Tokyo, Japan) as described in section 1-2-5.

2-2-8. DSC

A DSC Q 1000 (TA Instruments, New Castle, DE, USA) was used for DSC analysis as described in section 1-2-6.

2-2-9. Polarized light microscopy (PLM)

CsA samples were dispersed in silicone oil, and then their PLM images were taken with a CX41 microscope (Olympus, Tokyo, Japan).

2-2-10. Dissolution test

Dissolution testing on CsA samples was performed in 100 mL of distilled water. The dissolution medium was stirred at 100 rpm using a magnetic stirrer SST-66 (Shimadzu, Kyoto, Japan) at 37°C. Amorphous CsA and ASD/CsA powders (ca. 3 mg-CsA) were weighed and added into the glass beaker with 100 mL of water. Samples (400 μL) were collected and centrifuged at 10,000 rpm for 5 min. For the determination of CsA concentration, the supernatants diluted with acetonitrile were subjected to UPLC analysis as described in section 1-2-2.

2-2-11. Pharmacokinetic study

Male sprague-dawley rats, weighing 200–350 g (7–9 weeks of age; Japan SLC, Shizuoka, Japan), were housed as described in section 1-2-8.

Each CsA sample was suspended in 1 mL of distilled water, and it was orally administered at a dose of 10 mg-CsA/kg in rats. CsA was dissolved in DMSO, and the CsA solution at a dose of 0.5 mg/kg was intravenously administered in rats. After administration of CsA samples, 400 μL of blood samples was collected from the tail veins of rats at various periods. The collected blood samples were centrifuged at 10,000×*g* for 10 min, and the

supernatants were stored below –20°C until analysis. The plasma concentration of CsA and the pharmacokinetic parameters were determined as described in section 1-2-8.

2-2-12. Physicochemical stability

The stability study on the ASD/CsA was conducted at 40°C/75% relative humidity (RH) in open condition up to 4 weeks. The saturated salt solution method with sodium chloride was employed to obtain appropriate RH conditions, and aged samples were subjected to the UPLC analysis and dissolution testing.

2-2-13. Statistical analysis

For statistical comparisons, one-way analysis of variance with pairwise comparison by Fisher's LSD procedure was used (Statcel3, The Publisher OSM Ltd., Saitama, Japan). A P value of < 0.05 was considered significant for all analyses.

2-3 Results and discussion

2-3-1. Appearance of ASD formulations

In the present study, the FDD process was employed to produce the ASD/CsA with HPC-SSL, and the overall yield was over 80%. The obtained ASD/CsA was visualized by a SEM observation to clarify its morphology (Fig. 9). Amorphous CsA and spray-dried ASD formulation were also observed for comparison. The SEM image on amorphous CsA exhibited irregularly shaped powders with various particle sizes (Fig. 9A). On the other hand, spray-drying or FDD process resulted in clear change in morphology of CsA. Interestingly, the morphology of spray-dried ASD particles was also different from that of ASD/CsA prepared with the FDD process. The spray-dried ASD formulation existed as irregularly shaped particles with a rough surface (Fig. 9B). Non-uniform surface of spray-dried ASD formulation might be partly due to aggregation of particles during spray drying process. However, the FDD process produced uniform spherical ASD particles with smooth surface according to the result from the SEM observation (Fig. 9C).

2-3-2. Particle properties of ASD formulations

The particle properties of ASD formulations were characterized with a focus on particle size, bulk density, and flowability. Laser diffraction analysis demonstrated that the particle size distribution of ASD/CsA was much narrower than that of spray-dried ASD formulation (Fig. 10). The median size and SPAN of spray-dried ASD formulation were found to be 2.6 μm and 3.0, respectively (Table 5). The median size of ASD/CsA was 3.6 μm, and the SPAN was calculated to be 0.4. Thus, the FDD process could generate ASD formulation with uniform particle size compared with spray-drying technology under at least the present conditions.

(A)

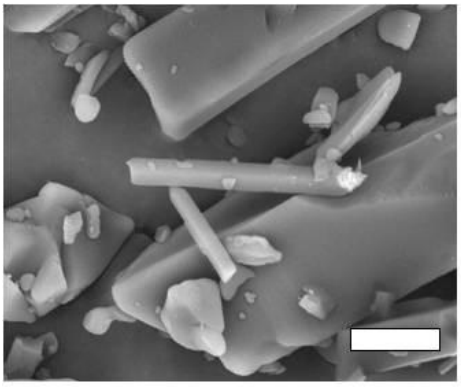

(B)

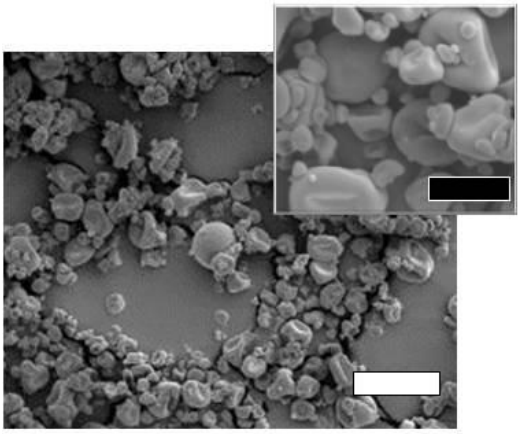

(C)

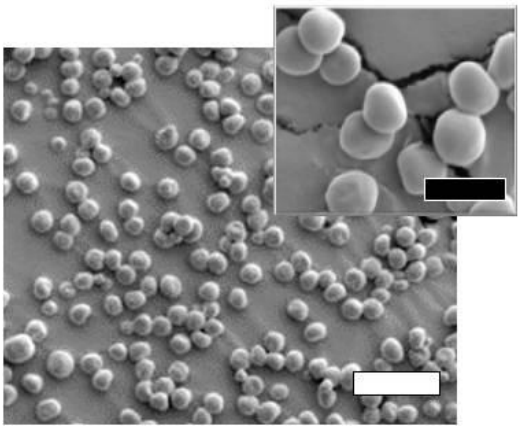

Fig. 9 SEM images of CsA samples, including (A) amorphous CsA, (B) spray-dried ASD/CsA, and (C) ASD/CsA prepared with FDD process. The inserts highlight the surface of ASD formulations. White and black bars represent 10 and 5 μm, respectively.

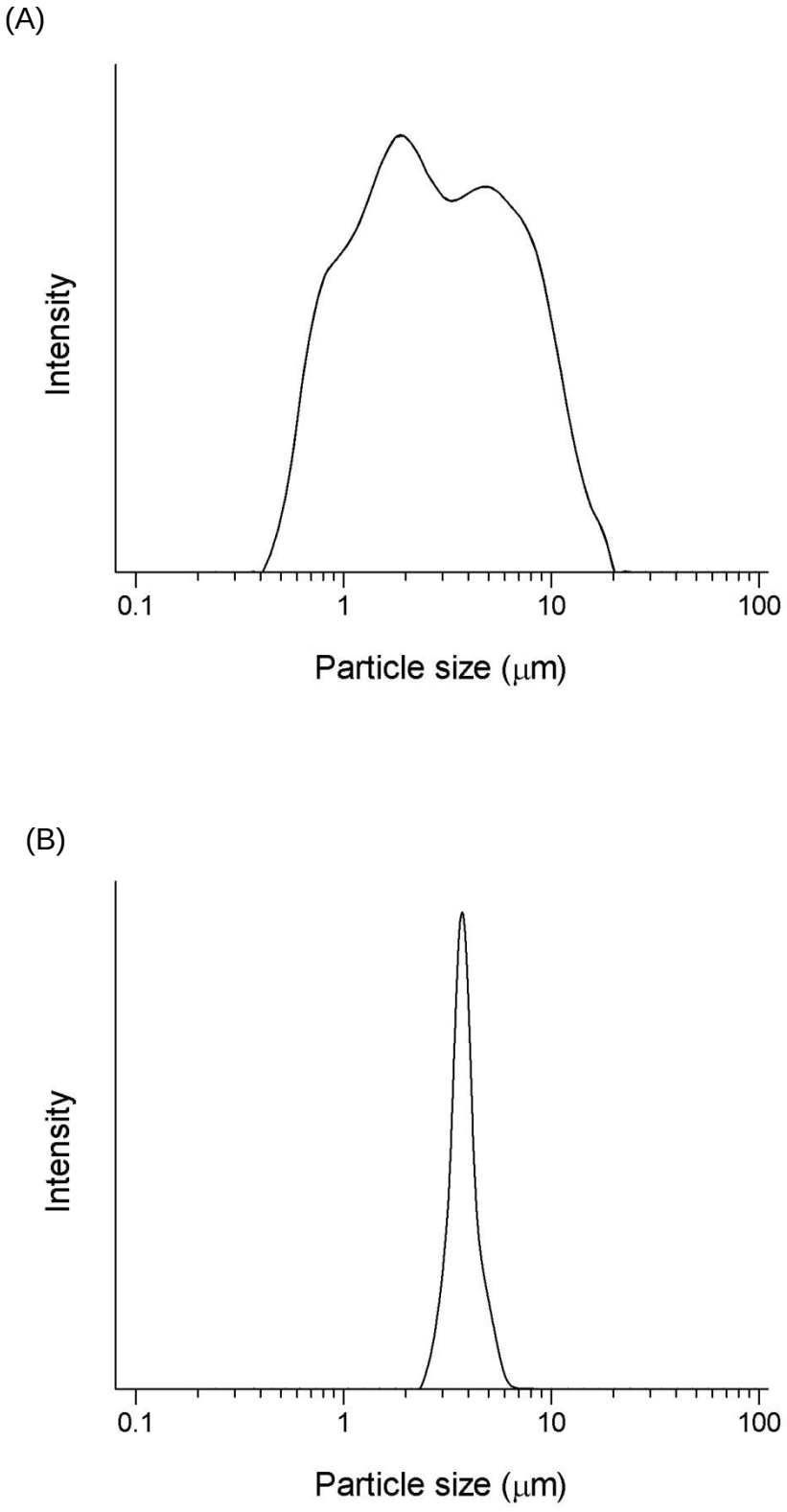

Fig. 10 Particle size distribution of (A) spray-dried ASD/CsA and (B) ASD/CsA prepared with FDD process.

The bulk density and flowability were also compared for both ASD formulations (Table 5). These parameters of spray-dried ASD formulation were calculated to be 0.2 g/mL and 11.3 mg/s, respectively. ASD/CsA showed better particle properties than spray-dried ASD formulation as evidenced by 0.3 g/mL of bulk density and 16.2 mg/s of flowability. Spherical shape, smooth surface, and narrow size distribution of powders can lead to the fine flow property because of the small contact area in the powder bed [68, 69]. The 2-fluid nozzle uses strong energy for generation of fine droplets, and so it may be challenging to strict control the droplet size [70]. In contrast, the inkjet head employed for the FDD process can continuously create uniform droplets by stable vibration energy, partly contributing to preparation of uniform particles. Therefore, the spherical form and uniform particle size of ASD/CsA prepared by FDD process could result in better fluidity than spray-dried particles. On the basis of these results, FDD process could provide ASD/CsA with desirable powder characteristics, and the fine and uniform ASD formulation might show improved dissolution behavior of CsA.

Table 5 Particle properties of ASD formulations

Preparation process	d_{10} (μm)	d_{50} (μm)	d_{90} (μm)	SPAN	Bulk density (g/mL)	Flowability (mg/s)
Spray-drying	0.8	2.6	8.4	3.0	0.2	11.3
FDD process	2.9	3.6	4.5	0.4	0.3	16.2

The d_{10}, d_{50}, and d_{90} are the particle diameters at 10%, 50%, and 90% of cumulative volume, respectively. SPAN = $(d_{90} - d_{10})/d_{50}$.

2-3-3. Crystallinity of ASD/CsA

XRPD and DSC analyses were conducted to evaluate the crystallinity of CsA within the formulation (Fig. 11). The XRPD patterns of crystalline CsA show several intense peaks, whereas the typical peaks for the crystalline form were found to be negligible in the amorphous CsA and ASD/CsA (Fig. 11A). The thermal behavior of CsA samples was evaluated to further characterize the physical state of CsA in ASD/CsA (Fig. 11B). In the DSC thermogram, crystalline CsA and amorphous CsA produced large endothermic peaks at 105°C and 125°C, respectively. The change in endothermic peak was attributable to phase transition of CsA [59]. In contrast, no endothermic peak was observed for the ASD/CsA in the examined temperature range. The ASD technology can provide stable amorphous drug formulations *via* interaction of drug and polymer [71]. According to the result from DSC analysis, interaction of CsA and HPC-SSL in the ASD formulation could contribute to prevention of molecular mobility during thermal analysis, inhibiting the phase transition of CsA. In addition to XRPD and DSC analyses, PLM observation was conducted because of its high detection sensitivity for crystallinity evaluation (Fig. 12). The PLM image on crystalline CsA reveals intense birefringence, whereas no birefringence in the PLM images of amorphous CsA and ASD/CsA was observed, suggesting an amorphous state of CsA in ASD/CsA. The result from PLM experiment was almost identical to that from XRPD and DSC analyses, and so ASD/CsA would contain amorphous CsA.

(A)

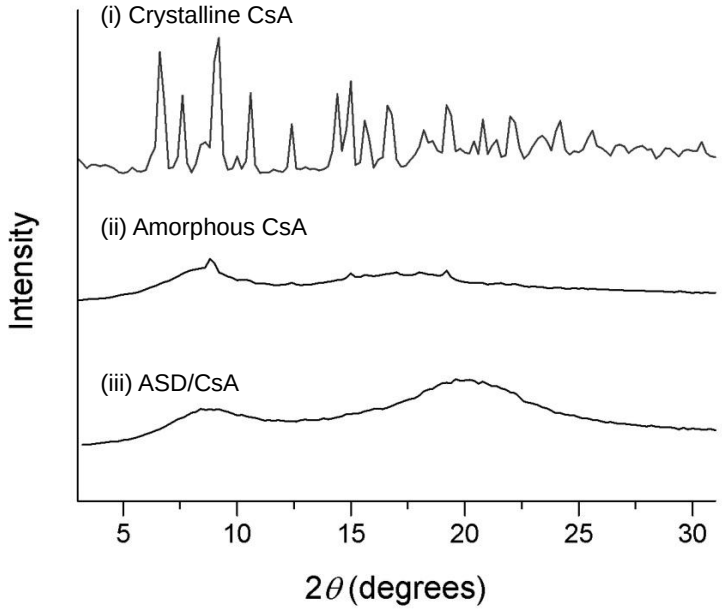

(B)

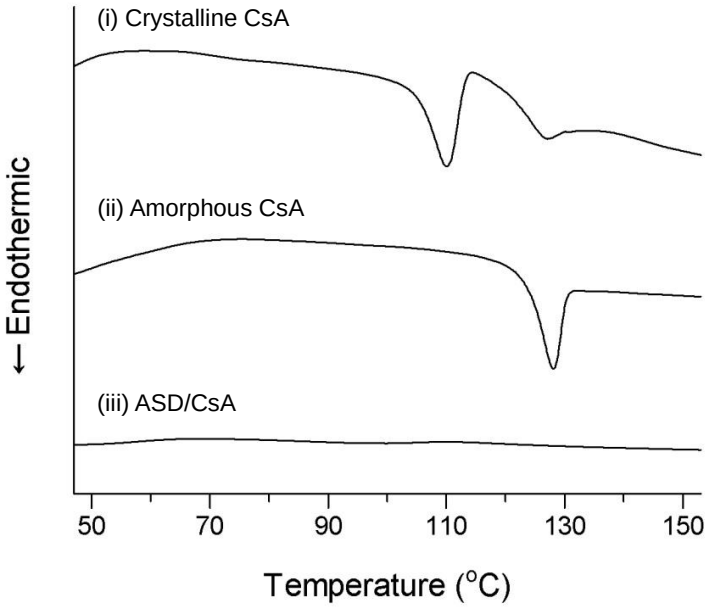

Fig. 11 Crystallinity of CsA in ASD/CsA by (A) XRPD and (B) DSC analyses. (i) Crystalline CsA, (ii) amorphous CsA, (iii) ASD/CsA.

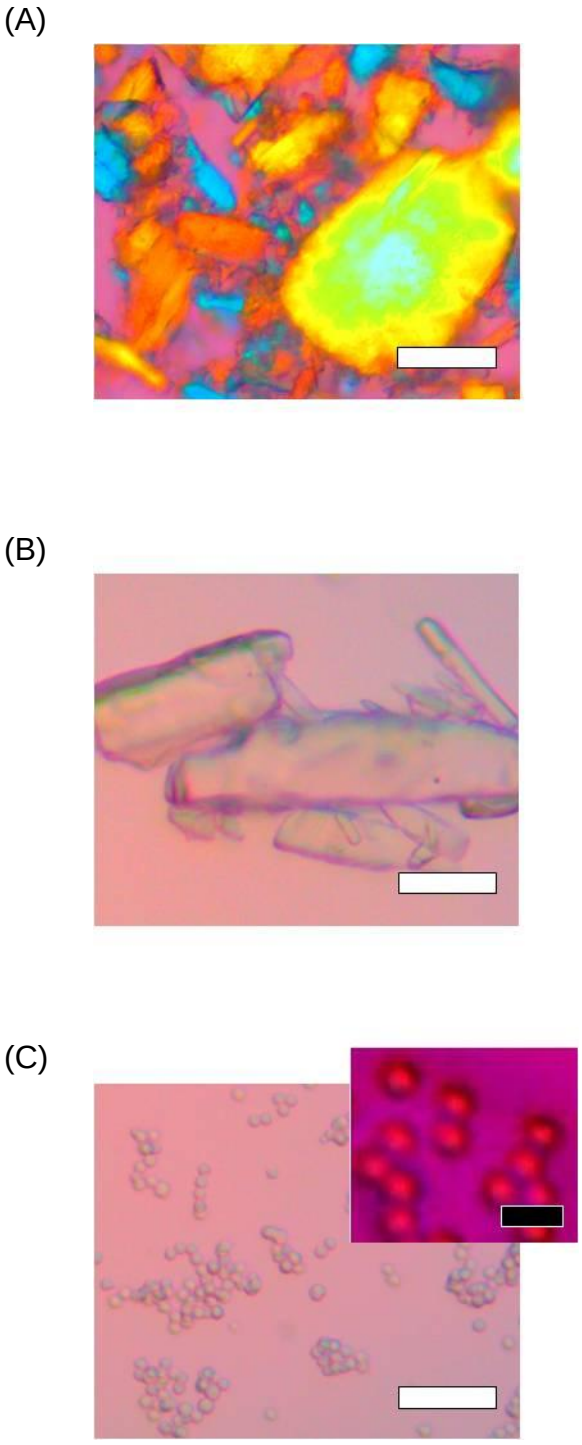

Fig. 12 PLM images of (A) crystalline CsA, (B) amorphous CsA, and (C) ASD/CsA. The insert is an enlarged PLM image of ASD/CsA. White and black bars represent 50 and 5 μm, respectively.

2-3-4. Dissolution behavior of ASD/CsA

To clarify the dissolution behavior of ASD/CsA, dissolution testing was performed in water for up to 60 min (Fig. 13). For amorphous CsA, the dissolved CsA concentration was ca. 60 ng/mL even after 60 min, and the highly limited dissolution behavior of CsA was observed in distilled water. However, the concentration of dissolved CsA was elevated up to 12 μg/mL for ASD/CsA, demonstrating significant improvement in the dissolution behavior of CsA upon ASD approach employing FDD process. Interestingly, the ASD/CsA appeared to offer constant drug release with pseudo-zero-order release kinetics. Dissolution behavior of drug particles is influenced by particle properties, such as the density, shape, and particle size. The extended drug release has been seen for drug particles with smooth surface and a regular spherical shape [72]. On the other hand, irregularity in the shape accelerates the dissolution rate of drugs by an increase in the surface areas. According to the mechanism of FDD process for preparing powder formulations, resultant formulations could be rigid particles. On the basis of the results from particle analyses, taken together with the principle of the FDD process, the constant drug release of the ASD/CsA could be potentially explained by particle properties, such as high density and uniform spherical particles. From the strong correlation with dissolution and absorption of CsA, drug release from ASD/CsA with pseudo-zero-order kinetics might contribute to the prolonged systemic exposure of CsA.

2-3-5. Pharmacokinetic behavior of ASD/CsA

The pharmacokinetic study in rats was conducted for orally-dosed amorphous CsA and ASD/CsA (10 mg-CsA/kg) to clarify the possible enhancement in oral BA of CsA by the ASD approach with the FDD process (Fig. 14 and Table 6). Oral administration of amorphous CsA in rats resulted in slow elevation of plasma CsA concentration and the limited systemic exposure. The C_{max} and $AUC_{0-inf.}$ were 0.1 μg/mL and 0.6 μg·h/mL, respectively.

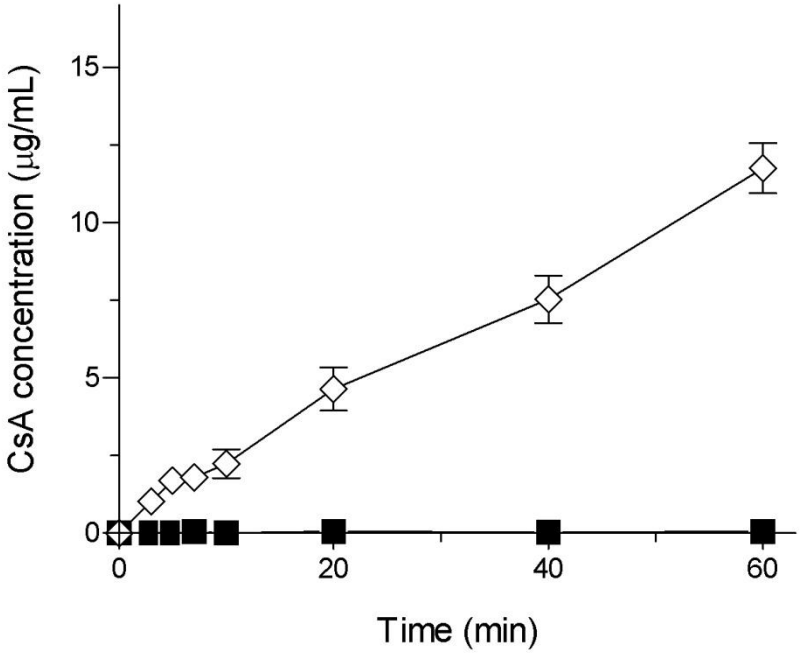

Fig. 13 Dissolution behavior of CsA samples, including amorphous CsA (■) and ASD/CsA (◇), in distilled water. Data represent mean±S.E. of 3 experiments.

On the other hand, orally-dosed ASD/CsA provided high systemic exposure of CsA compared with amorphous CsA, and each C_{max} and $AUC_{0-inf.}$ value was 1.1 μg/mL and 11.4 μg·h/mL, respectively. There was ca. 18-fold enhancement in the oral BA of CsA for ASD/CsA with BA of 12.8% compared with amorphous CsA with BA of 0.7%. The $T_{1/2}$ was different between ASD/CsA and amorphous CsA, and the extended plasma concentration of CsA was observed after oral administration of the ASD/CsA. The prolongation of plasma CsA level was attributable to the controlled drug release from the ASD/CsA. The controlled drug delivery system can provide prolonged duration of action, offering reduced frequency of dosing and improved patient compliance [73]. The CV in $AUC_{0-inf.}$ for orally-dosed amorphous CsA and ASD/CsA was calculated to be ca. 50% and 20%, respectively. Therefore, the variation in oral absorption of CsA was suppressed for ASD/CsA. The uniformly-shaped ASD/CsA with fairly narrow size distribution could provide reproducible

release of CsA in GI tract, possibly resulting in the consistent oral absorption. Consistent absorption of CsA is needed for stable therapeutic effects since the unpredictable absorption often causes treatment failure due to the insufficient blood level with below therapeutic concentration of CsA. Application of FDD process to development of ASD/CsA could be a promising strategy to offer favorable oral absorption of CsA with prolonged systemic exposure and low variability.

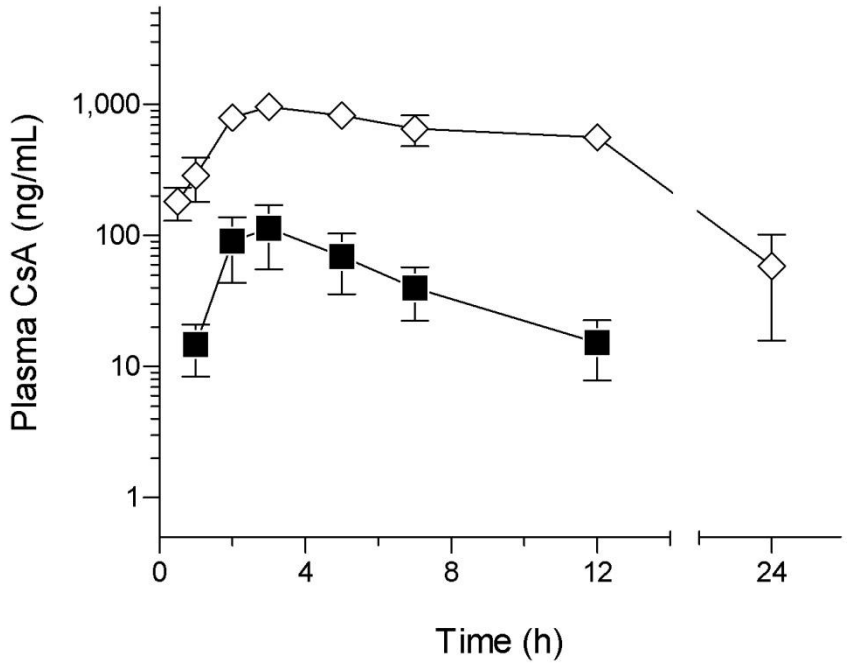

Fig. 14 Plasma concentration-time profiles of CsA after oral administration of CsA samples (10 mg-CsA/kg) in rats. ■, amorphous CsA and ◇, ASD/CsA. Data represents mean±S.E. of 4–5 experiments.

Table 6 Pharmacokinetic parameters of CsA after administration of CsA samples

	C_{max} (μg/mL)	$T_{1/2}$ (h)	$AUC_{0-inf.}$ (μg· h/mL)	BA (%)
Amorphous CsA	0.1±0.1	2.4±0.2	0.6±0.3	0.7
ASD/CsA	1.1±0.1**	4.7±1.0*	11.4±2.3**	12.8

C_{max}, maximum concentration; $T_{1/2}$, half-life time; $AUC_{0-inf.}$, area under the curve of plasma concentration *versus* time from t=0 to t=infinity; and BA, bioavailability. Data represents mean±S.E. of 5–6 experiments. *, $P<0.05$ and **, $P<0.01$ with respect to amorphous CsA.

2-3-6. Physicochemical stability of ASD/CsA

Physicochemical stability testing on the ASD/CsA was carried out with a focus on the purity and dissolution of CsA. The ASD/CsA was stored at 40°C/75% RH for up to 4 weeks. In UPLC analysis, no significant degradation of CsA in ASD/CsA was seen even after storage under accelerated conditions (Fig. 15). However, ca. 60% reduction in the dissolution of CsA was observed after storage of the ASD/CsA under accelerated conditions for 2 weeks. No significant difference in the reduction of CsA dissolution was observed between 2 and 4 weeks of storage. The ASD formulation can be classified into a one-phase or two-phase system depending on the molecular arrangement. The one-phase ASD system has been reported to be changed into the two-phase ASD system during storage at 40°C/75% RH, leading to reduction of the dissolution behavior [74]. Since the ASD/CsA would be identified as a one-phase ASD system according to the principle of the FDD process, the impaired drug release from aged ASD/CsA could be partly explained by the aggregation of CsA molecules in the ASD/CsA particles. Surrounding high humidity causes decrease in the glass transition temperature of the ASD, facilitating the particle aggregation and the phase transition [75]. Therefore, use of protection packages, such as press through package and strip package, is needed for maintain the dissolution property of the ASD/CsA.

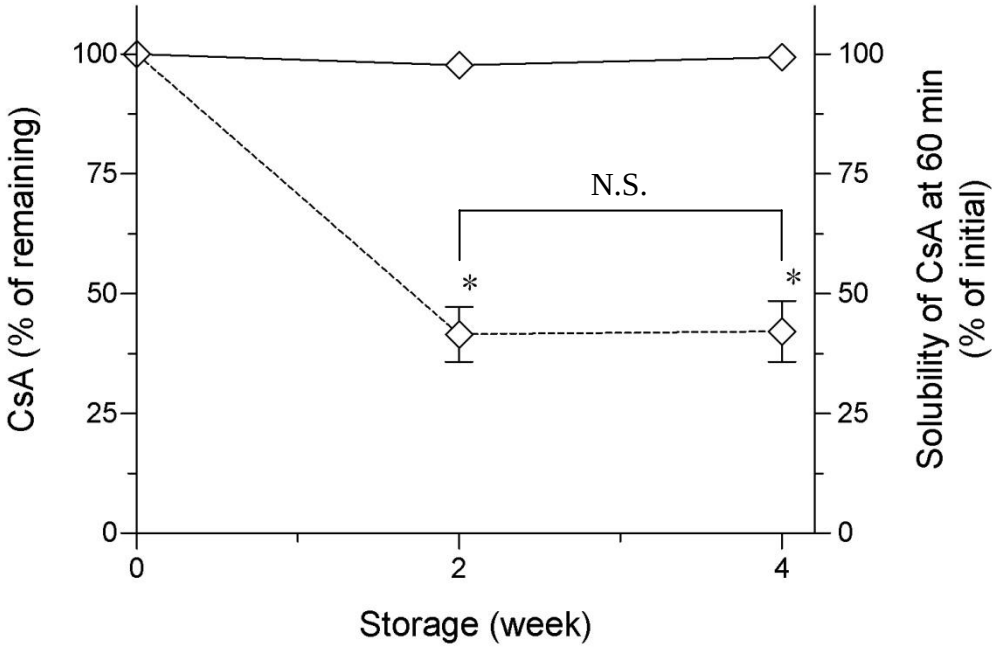

Fig. 15 Stability data on ASD/CsA. The ASD/CsA was stored at 40°C/75% RH for the indicated period. Solid line, the purity (% of remaining) of CsA was determined by UPLC analysis; and dashed line, the release CsA (% of initial) from the ASD/CsA at 60 min was plotted over the storage periods. Data represents mean±S.E. of 4–5 experiments. N.S., not statistically significant. *, $P < 0.05$ with respect to freshly prepared ASD/CsA (0 week).

2-4 Conclusion

FDD process successfully provided spherical ASD/CsA particles with narrow size distribution. In comparison with spray-dried ASD particles, ASD/CsA had better particle properties. ASD/CsA significantly improved dissolution behavior of CsA compared with amorphous CsA, and the dissolution pattern was pseudo-zero order release. Orally-dosed ASD/CsA provided higher systemic exposure of CsA in rats than that of amorphous CsA. Oral administration of ASD/CsA resulted in prolongation of the $T_{1/2}$ compared with that of amorphous CsA, and the extended systemic exposure was attributable to the dissolution behavior of ASD/CsA with pseudo-zero order kinetics. From these findings, ASD/CsA prepared with FDD process employing inkjet head could be a beneficial dosage form for CsA with sustained systemic exposure, contributing to the prolonged duration of the pharmacological actions.

Summary and conclusion

CsA exerts potent immunosuppressive effects by inhibition of calcineurin, and the efficacy is strongly correlated with the blood concentration. However, oral absorption of CsA is often poor and variable due to the limited dissolution in GI tract. Improvement in pharmacokinetic behavior of CsA after the oral administration is required to obtain the better therapeutic effects. The present study aimed to control pharmacokinetic behavior of CsA by modification of the physicochemical properties.

In chapter 1, nCsA and nCsA/MAN was prepared by FNP using MIVM and spray-drying to obtain rapid oral absorption of CsA. Both nCsA and nCsA/MAN was micron-sized aggregates and reconstituted nanoparticles of CsA in distilled water. Dissolution behavior of nCsA/MAN was better than that of nCsA, demonstrating the efficiency of mannitol as a matrix former. Oral administration of nCsA/MAN resulted in high and consistent absorption of CsA in rats. From these results, combined approach of FNP and spray-drying could be efficacious to improve systemic exposure of CsA. In particular, nCsA/MAN could be a beneficial dosage form of CsA to offer the rapid oral absorption with low variability.

In chapter 2, ASD/CsA was obtained by FDD process for enhancement in the oral absorption. FDD process provided spherical ASD particles with uniform shape and narrow size distribution. ASD/CsA showed fine dissolution behavior with pseudo-zero-order release kinetics. Orally-dosed ASD/CsA offered higher systemic exposure of CsA in rats than amorphous CsA, and there appeared to prolong the systemic exposure for ASD/CsA due to the constant drug release behavior. The present study demonstrated that the applicability of FDD process for preparation method of ASD formulation, and ASD/CsA might be an effective dosage form of CsA with constant drug release and sustained systemic exposure.

Each CsA formulation had a different absorption property, such as rapid oral absorption and prolonged systemic exposure. From the correlation of CsA action and the blood concentration, faster oral absorption of CsA could contribute to the potent pharmacological actions. ASD/CsA with sustained systemic exposure could offer the prolonged duration of the action. The dosing amount of CsA depends on types of transplant and the patient's conditions, and the blood concentration must be maintained within the recommended target range. Therefore, an appropriate choice of CsA formulations should be conducted to obtain desirable clinical outcomes.

From these findings, pharmacokinetic control of CsA was achieved by FNP technology with MIVM and FDD process. In conclusion, both nCsA/MAN and ASD/CsA might be suitable dosage forms of CsA to provide the improved therapeutic effects.

Acknowledgements

I would like to express my sincere thanks to Prof. Satomi Onoue at University of Shizuoka for supporting this work and my school life.

I am deeply grateful to Prof. Hak-Kim Chan in Advanced Drug Delivery Group at The University of Sydney and Prof. Robert K. Prud'homme in Department of Chemical and Biological Engineering at Princeton University for invaluable comments and discussions.

I am greatly indebted to Prof. Naoto Oku in Department of Medical Biochemistry, Prof. Hiroshi Hashimoto in Laboratory of Physical Biochemistry, and Dr. Shinya Uchida in Department of Pharmacy Practice and Science at the University of Shizuoka for their valuable suggestions and fruitful comments.

I thank Dr. Yoshiki Seto and Dr. Hideyuki Sato at the University of Shizuoka, for giving me helpful comments and warm encouragement through this study.

I also thank Dr. Jennifer Wong in Advanced Drug Delivery Group at The University of Sydney and everyone in the Department of Pharmacokinetics and Pharmacodynamics at the University of Shizuoka for their technical support. I thank ILS Inc. for providing CsA. I thank Nagai Memorial Research Scholarship from the Pharmaceutical Society of Japan.

Finally, I would like to express my deepest gratitude to my family for supporting my school life.

March, 2018

Hiroki Suzuki

References

1. A. Czogalla, Oral cyclosporine A--the current picture of its liposomal and other delivery systems, *Cell Mol Biol Lett*, **14**: 139–152 (2009).
2. N. Kamar, J. Allard, J.L. Ader, L. Rostaing, Cyclosporine-A-based immunosuppression and renal functional reserve in organ-transplant patients, *Transplant Proc*, **36**: 248s–250s (2004).
3. D. Tedesco, L. Haragsim, Cyclosporine: a review, *J Transplant*, **2012**: 1–7 (2012).
4. J.F. Borel, C. Feurer, H.U. Gubler, H. Stahelin, Biological effects of cyclosporin A: a new antilymphocytic agent, *Agents Actions*, **43**: 179–186 (1976).
5. A. Lawen, Biosynthesis and mechanism of action of cyclosporins, *Prog Med Chem*, **33**: 53–97 (1996).
6. R.M. Wenger, Synthesis of Cyclosporine .3. Total Syntheses of Cyclosporin-a and Cyclosporin-H, 2 Fungal Metabolites Isolated from the Species Tolypocladium-Inflatum Gams, *Helv Chim Acta*, **67**: 502–525 (1984).
7. A. Schumacher, A. Nordheim, Progress towards a molecular understanding of cyclosporin A-mediated immunosuppression, *Clin Investig*, **70**: 773–779 (1992).
8. D.J. Freeman, Pharmacology and pharmacokinetics of cyclosporine, *Clin Biochem*, **24**: 9–14 (1991).
9. S.A. Survase, L.D. Kagliwal, U.S. Annapure, R.S. Singhal, Cyclosporin A--a review on fermentative production, downstream processing and pharmacological applications, *Biotechnol Adv*, **29**: 418–435 (2011).
10. A. Pawarode, P.K. Wallace, L.A. Ford, M. Barcos, M.R. Baer, Long-term safety and efficacy of cyclosporin A therapy for T-cell large granular lymphocyte leukemia, *Leuk Lymphoma*, **51**: 338–341 (2010).

11. D. Lulic, J. Burns, E.C. Bae, H. van Loveren, C.V. Borlongan, A Review of Laboratory and Clinical Data Supporting the Safety and Efficacy of Cyclosporin A in Traumatic Brain Injury, *Neurosurgery*, **68**: 1172–1185 (2011).

12. M.M. Osman, D. Lulic, L. Glover, C.E. Stahl, T. Lau, H. van Loveren, C.V. Borlongan, Cyclosporine-A as a neuroprotective agent against stroke: Its translation from laboratory research to clinical application, *Neuropeptides*, **45**: 359–368 (2011).

13. E. Nizankowska, J. Soja, G. Pinis, G. Bochenek, K. Sladek, B. Domagala, A. Pajak, A. Szczeklik, Treatment of steroid-dependent bronchial asthma with cyclosporin, *Eur Respir J*, **8**: 1091–1099 (1995).

14. A. Ready, Experience with cyclosporine, *Transplant Proc*, **36**: 135S–138S (2004).

15. C.Y. Wu, L.Z. Benet, M.F. Hebert, S.K. Gupta, M. Rowland, D.Y. Gomez, V.J. Wacher, Differentiation of absorption and first-pass gut and hepatic metabolism in humans: studies with cyclosporine, *Clin Pharmacol Ther*, **58**: 492–497 (1995).

16. P.A. Kelly, H. Wang, K.L. Napoli, B.D. Kahan, H.W. Strobel, Metabolism of cyclosporine by cytochromes P450 3A9 and 3A4, *Eur J Drug Metabol Pharmacokinet*, **24**: 321–328 (1999).

17. G. Fricker, J. Drewe, J. Huwyler, H. Gutmann, C. Beglinger, Relevance of p-glycoprotein for the enteral absorption of cyclosporin A: in vitro-in vivo correlation, *Br J Pharmacol*, **118**: 1841–1847 (1996).

18. S.K. Gupta, R.C. Manfro, S.J. Tomlanovich, J.G. Gambertoglio, M.R. Garovoy, L.Z. Benet, Effect of food on the pharmacokinetics of cyclosporine in healthy subjects following oral and intravenous administration, *J Clin Pharmacol*, **30**: 643–653 (1990).

19. U.I. Schwarz, P.E. Johnston, D.G. Bailey, R.B. Kim, G. Mayo, A. Milstone, Impact of citrus soft drinks relative to grapefruit juice on ciclosporin disposition, *Br J Clin*

Pharmacol, **62**: 485–491 (2006).

20. G.C. Yee, T.P. Lennon, D.J. Gmur, M.S. Kennedy, H.J. Deeg, Age-dependent cyclosporine: pharmacokinetics in marrow transplant recipients, *Clin Pharmacol Ther*, **40**: 438–443 (1986).

21. C. Misteli, E. Rey, G. Pons, M.O. Richard, P. d'Athis, A. Legrand, P. Bougneres, G. Olive, Pharmacokinetics of oral cyclosporin A in diabetic children and adolescents, *Eur J Clin Pharmacol*, **38**: 181–184 (1990).

22. K.R. Schultz, T.J. Nevill, R.F. Balshaw, C.L. Toze, T. Corr, C.J. Currie, D.K. Strong, P.A. Keown, Effect of gastrointestinal inflammation and age on the pharmacokinetics of oral microemulsion cyclosporin A in the first month after bone marrow transplantation, *Bone Marrow Transplant*, **26**: 545–551 (2000).

23. N.K. Wadhwa, T.J. Schroeder, E. O'Flaherty, A.J. Pesce, S.A. Myre, M.R. First, The effect of oral metoclopramide on the absorption of cyclosporine, *Transplant Proc*, **19**: 1730–1733 (1987).

24. V. Garg, R. van Heeswijk, J.E. Lee, K. Alves, P. Nadkarni, X. Luo, Effect of telaprevir on the pharmacokinetics of cyclosporine and tacrolimus, *Hepatology*, **54**: 20–27 (2011).

25. M.F. Hebert, J.P. Roberts, T. Prueksaritanont, L.Z. Benet, Bioavailability of cyclosporine with concomitant rifampin administration is markedly less than predicted by hepatic enzyme induction, *Clin Pharmacol Ther*, **52**: 453–457 (1992).

26. S.G. Pollard, Pharmacologic monitoring and outcomes of cyclosporine, *Transplant P*, **36**: 404s–407s (2004).

27. M. Guada, A. Beloqui, M.N. Kumar, V. Preat, C. Dios-Vieitez Mdel, M.J. Blanco-Prieto, Reformulating cyclosporine A (CsA): More than just a life cycle management strategy, *J Control Release*, **225**: 269–282 (2016).

28. C.J. Dunn, A.J. Wagstaff, C.M. Perry, G.L. Plosker, K.L. Goa, Cyclosporin: an updated review of the pharmacokinetic properties, clinical efficacy and tolerability of a microemulsion-based formulation (neoral)1 in organ transplantation, *Drugs*, **61**: 1957–2016 (2001).

29. M. Guada, A. Beloqui, N.V.R. Kumar, V. Preat, M.D. Dios-Vieitez, M.J. Blanco-Prieto, Reformulating cyclosporine A (CsA): More than just a life cycle management strategy, *J Control Release,* **225**: 269–282 (2016).

30. S. Onoue, H. Sato, K. Ogawa, Y. Kawabata, T. Mizumoto, K. Yuminoki, N. Hashimoto, S. Yamada, Improved dissolution and pharmacokinetic behavior of cyclosporine A using high-energy amorphous solid dispersion approach, *Int J Pharm*, **399**: 94–101 (2010).

31. V. Hirunpanich, H. Sato, Improvement of cyclosporine A bioavailability by incorporating ethyl docosahexaenoate in the microemulsion as an oil excipient, *Eur J Pharm Biopharm*, **73**: 247–252 (2009).

32. J. Deng, Z. Zhang, C. Liu, L. Yin, J. Zhou, H. Lv, The studies of N-Octyl-N-Arginine-Chitosan coated liposome as an oral delivery system of Cyclosporine A, *Journal Pharm Pharmacol*, **67**: 1363–1370 (2015).

33. P. Guan, Y. Lu, J. Qi, W. Wu, Readily restoring freeze-dried probilosomes as potential nanocarriers for enhancing oral delivery of cyclosporine A, *Colloid Surf B Biointerfaces*, **144**: 143–151 (2016).

34. H. Yu, D. Xia, Q. Zhu, C. Zhu, D. Chen, Y. Gan, Supersaturated polymeric micelles for oral cyclosporine A delivery, *Eur J Pharm Biopharm*, **85**: 1325–1336 (2013).

35. J. Dai, T. Nagai, X. Wang, T. Zhang, M. Meng, Q. Zhang, pH-sensitive nanoparticles for improving the oral bioavailability of cyclosporine A, *Int J Pharm*, **280**: 229–240 (2004).

36. S. Onoue, H. Suzuki, Y. Kojo, S. Matsunaga, H. Sato, T. Mizumoto, K. Yuminoki, N. Hashimoto, S. Yamada, Self-micellizing solid dispersion of cyclosporine A with improved dissolution and oral bioavailability, *Eur J Pharm Sci*, **62**: 16–22 (2014).

37. K. Miyake, H. Arima, T. Irie, F. Hirayama, K. Uekama, Enhanced absorption of cyclosporin A by complexation with dimethyl-beta-cyclodextrin in bile duct-cannulated and -noncannulated rats, *Biol Pharm Bull*, **22**: 66–72 (1999).

38. H. Cho, Y. Chung, Water soluble cyclosporine monomethoxy poly(ethyleneglycol) conjugates as potential prodrugs, *Arch Pharm Res*, **27**: 662–669 (2004).

39. R. Ghadi, N. Dand, BCS class IV drugs: Highly notorious candidates for formulation development, *J Control Release*, **248**: 71–95 (2017).

40. K. Sigfridsson, A.J. Lundqvist, M. Strimfors, Particle size reduction for improvement of oral absorption of the poorly soluble drug UG558 in rats during early development, *Drug Dev Ind Pharm*, **35**: 1479–1486 (2009).

41. J.J. Guo, P.F. Yue, J.L. Lv, J. Han, S.S. Fu, S.X. Jin, S.Y. Jin, H.L. Yuan, Development and in vivo/in vitro evaluation of novel herpetrione nanosuspension, *Int J Pharm*, **441**: 227–233 (2013).

42. B. Sinha, R.H. Muller, J.P. Moschwitzer, Bottom-up approaches for preparing drug nanocrystals: formulations and factors affecting particle size, *Int J Pharm*, **453**: 126–141 (2013).

43. J.P. Moschwitzer, Drug nanocrystals in the commercial pharmaceutical development process, *Int J Pharm*, **453**: 142–156 (2013).

44. R. Shegokar, R.H. Muller, Nanocrystals: industrially feasible multifunctional formulation technology for poorly soluble actives, *Int J Pharm*, **399**: 129–139 (2010).

45. C.M. Keck, R.H. Muller, Drug nanocrystals of poorly soluble drugs produced by

high pressure homogenisation, *Eur J Pharm Biopharm*, **62**: 3–16 (2006).

46. S.M. D'Addio, R.K. Prud'homme, Controlling drug nanoparticle formation by rapid precipitation, *Adv Drug Deliv Rev*, **63**: 417–426 (2011).

47. Y. Liu, C.Y. Cheng, Y. Liu, R.K. Prud'homme, R.O. Fox, Mixing in a multi-inlet vortex mixer (MIVM) for flash nano-precipitation, *Chem Eng Sci*, **63**: 2829–2842 (2008).

48. S.F. Chow, C.C. Sun, A.H. Chow, Assessment of the relative performance of a confined impinging jets mixer and a multi-inlet vortex mixer for curcumin nanoparticle production, *Eur J Pharm Biopharm*, **88**: 462–471 (2014).

49. J. Jinno, N. Kamada, M. Miyake, K. Yamada, T. Mukai, M. Odomi, H. Toguchi, G.G. Liversidge, K. Higaki, T. Kimura, Effect of particle size reduction on dissolution and oral absorption of a poorly water-soluble drug, cilostazol, in beagle dogs, *J Control Release*, **111**: 56–64 (2006).

50. R.H. Muller, K. Peters, Nanosuspensions for the formulation of poorly soluble drugs - I. Preparation by a size-reduction technique, *Int J Pharmaceut*, **160**: 229–237 (1998).

51. S.M. Ansell, S.A. Johnstone, P.G. Tardi, L. Lo, S. Xie, Y. Shu, T.O. Harasym, N.L. Harasym, L. Williams, D. Bermudes, B.D. Liboiron, W. Saad, R.K. Prud'homme, L.D. Mayer, Modulating the therapeutic activity of nanoparticle delivered paclitaxel by manipulating the hydrophobicity of prodrug conjugates, *J Med Chem*, **51**: 3288–3296 (2008).

52. B.K. Johnson, R.K. Prud'homme, Flash NanoPrecipitation of organic actives and block copolymers using a confined impinging jets mixer, *Aust J Chem*, **56**: 1021–1024 (2003).

53. B.K. Johnson, R.K. Prud'homme, Mechanism for rapid self-assembly of block

copolymer nanoparticles, *Phys Rev Lett*, **91**: 110–121 (2003).

54. B.K. Johnson, W. Saad, R.K. Prud'homme, Nanoprecipitation of pharmaceuticals using mixing and block copolymer stabilization, *Acs Sym Ser*, **924**: 278–291 (2006).

55. Y. Liu, K. Kathan, W. Saad, R.K. Prud'homme, Ostwald ripening of beta-carotene nanoparticles, *Phys Rev Lett*, **98**: 36–44 (2007).

56. B. Gajra, C. Dalwadi, R. Patel, Formulation and optimization of itraconazole polymeric lipid hybrid nanoparticles (Lipomer) using box behnken design, *Daru*, **23**: 1–15 (2015).

57. V. Bertacche, E. Pini, R. Stradi, F. Stratta, Quantitative determination of amorphous cyclosporine in crystalline cyclosporine samples by Fourier transform infrared spectroscopy, *J Pharm Sci*, **95**: 159–166 (2006).

58. W.Y. Su, N. Jia, H.S. Li, H.X. Hao, C.L. Li, Polymorphism of D-mannitol: Crystal structure and the crystal growth mechanism, *Chinese J Chem Eng*, **25**: 358–362 (2017).

59. D. Lechuga-Ballesteros, A. Abdul-Fattah, C.L. Stevenson, D.B. Bennett, Properties and stability of a liquid crystal form of cyclosporine-the first reported naturally occurring peptide that exists as a thermotropic liquid crystal, *J Pharm Sci*, **92**: 1821–1831 (2003).

60. M. Kumon, P.C. Kwok, H. Adi, D. Heng, H.K. Chan, Can low-dose combination products for inhalation be formulated in single crystalline particles?, *Eur J Pharm Sci*, **40**: 16–24 (2010).

61. T. Takagi, C. Ramachandran, M. Bermejo, S. Yamashita, L.X. Yu, G.L. Amidon, A provisional biopharmaceutical classification of the top 200 oral drug products in the United States, Great Britain, Spain, and Japan, *Mol Pharm*, **3**: 631–643 (2006).

62. D. Horter, J.B. Dressman, Influence of physicochemical properties on dissolution of

drugs in the gastrointestinal tract, *Adv Drug Deliv Rev*, **46**: 75–87 (2001).

63. J. Sun, F. Wang, Y. Sui, Z. She, W. Zhai, C. Wang, Y. Deng, Effect of particle size on solubility, dissolution rate, and oral bioavailability: evaluation using coenzyme Q(1)(0) as naked nanocrystals, *Int J Nanomed*, **7**: 5733–5744 (2012).

64. R.J. Hintz, K.C. Johnson, The Effect of Particle-Size Distribution on Dissolution Rate and Oral Absorption, *Int J Pharmaceut*, **51**: 9–17 (1989).

65. Y. Norikane, H. Nakamura, S. Oogaki, H. Sekiguchi, Liquid droplet ejecting method, liquid droplet ejection apparatus, inkjet recording apparatus, production method of fine particles, fine particle production apparatus, and toner, Int Patent Appl No PCT/JP2011/057075 (2011).

66. B.C. Hancock, M. Parks, What is the true solubility advantage for amorphous pharmaceuticals?, *Pharm Res*, **17**: 397–404 (2000).

67. L.F. Huang, W.Q. Tong, Impact of solid state properties on developability assessment of drug candidates, *Adv Drug Deliv Rev*, **56**: 321–334 (2004).

68. M. Maghsoodi, How spherical crystallization improves direct tableting properties: a review, *Adv Pharm Bull*, **2**: 253–257 (2012).

69. J.S. Kaerger, S. Edge, R. Price, Influence of particle size and shape on flowability and compactibility of binary mixtures of paracetamol and microcrystalline cellulose, *Eur J Pharm Sci*, **22**: 173–179 (2004).

70. B. Bittner, T. Kissel, Ultrasonic atomization for spray drying: a versatile technique for the preparation of protein loaded biodegradable microspheres, *J Microencapsul*, **16**: 325–341 (1999).

71. S.L. Shimpi, B. Chauhan, K.R. Mahadik, A. Paradkar, Stabilization and improved in vivo performance of amorphous etoricoxib using Gelucire 50/13, *Pharm Res*, **22**: 1727–1734 (2005).

72. S. Onoue, M. Ochi, S. Yamada, Development of (-)-epigallocatechin-3-gallate (EGCG)-loaded enteric microparticles with intestinal mucoadhesive property, *Int J Pharm*, **410**: 111–113 (2011).

73. A. Nokhodchi, S. Raja, P. Patel, K. Asare-Addo, The role of oral controlled release matrix tablets in drug delivery systems, *BioImpacts : BI*, **2**: 175–187 (2012).

74. H. Sato, Y. Kawabata, K. Yuminoki, N. Hashimoto, Y. Yamauchi, K. Ogawa, T. Mizumoto, S. Yamada, S. Onoue, Comparative studies on physicochemical stability of cyclosporine A-loaded amorphous solid dispersions, *Int J Pharm*, **426**: 302–306 (2012).

75. F. Qian, J. Huang, M.A. Hussain, Drug-polymer solubility and miscibility: Stability consideration and practical challenges in amorphous solid dispersion development, *J Pharm Sci*, **99**: 2941–2947 (2010).